

## **Response to Reviewer #2**

*The authors would like to thank both reviewers for their comments and suggestions, which have helped to improve the quality of the manuscript. Please, find below a detailed response to the reviewer's comments.*

### **Comment:**

**The manuscript titled "Profiling of aerosol microphysical properties at several EARLINET/AERONET sites during 2012 ChArMEx/EMEP campaign" intends to analyze the microphysical properties of aerosols at five different lidar ground-based stations, and to use the results obtained for the validation of different mineral dust models.**

**The paper addresses an interesting and sound topic related to the aims of the ChArMEx campaign. The English language and presentation are very clear and up to the standard of an international journal. The figures and tables in the manuscript are also relevant.**

**The paper is well organised and detailed. I strongly appreciate the effort of the authors to compile different ground-based observations and models. In this sense, the authors present a nice description of the state of the atmosphere during the ChArMEx campaign (9-11 July 2012). This technical work is noticeable; but somehow does not importantly contribute to science. After having read carefully the paper, I am not feeling having learnt a lot, for the following reasons.**

**Most of the paper is devoted to the description of aerosol optical properties, aerosol mass and layering at different stations. The processes involved in the dynamics of transport of dust to the Mediterranean are widely known (as also stated by the authors in the references included). These processes were largely studied in a number of publications, such as Pey et al., 2013; Salvador et al., 2014; Gkikas et al., 2013 and 2015, Sicard et al., 2015; just to cite some recent papers. The models used (BSC-DREAM8b, NMMB/BSC-Dust, DREAM8-NMME, COSMO-MUSCAT) are not new either, and have been extensively validated in other studies (e.g. Perez et al., 2008; Pérez et al., 2011a, 2011b; Basart et al., 2012; Haustein et al., 2012; Mona et al., 2014, and especially, in Binietoglou et al., 2015, among many others). Also, using GARRLIC and LIRIC for retrieving microphysical properties is not a new contribution either.**

**Therefore, the authors should clarify which part of the manuscript is innovative and how this paper contributes to an advancement of the scientific knowledge.**

### **Response:**

The main contribution of this manuscript is the analysis of the microphysical properties, which has not been presented in the previous studies mentioned by the reviewer, mostly based on the analysis of the optical properties.

As far as LIRIC is concerned, results presented here follow a whole event during a continuous period of time in different stations operating simultaneously and thus providing vertical, horizontal and temporal coverage. Up to our knowledge, only the study by Chaikovsky et al. (2016) provides information about different lidars measuring simultaneously. However, those lidars were located at the same site for inter-

comparison purposes and the temporal evolution of the aerosol microphysical properties was not considered either. In studies other than Chaikovsky et al. (2016), LIRIC was applied to single sites with a single lidar and for specific selected case studies. In this sense, we show the capability of LIRIC to provide information about aerosol microphysical properties with a high vertical and temporal resolution in a simple, automated and robust way within a network such as EARLINET, providing regional coverage. The easy implementation of LIRIC in EARLINET/AERONET stations and the quality of the results obtained make it very suitable this kind of analysis within networks and during special campaigns. Additionally, information provided by LIRIC in such scenarios could be used to test and improve the performance of dust and aerosol forecast models.

In previous studies, models have been mostly validated using optical and column-integrated properties, but not many validations of the microphysical properties profiles are available, except for the study by Biniotoglou et al. (2015). Our study goes one step further than the one by Biniotoglou in the sense that the same dust event is evaluated regionally and we include also an evaluation of the temporal evolution at Granada station. Biniotoglou et al. (2015) is a comprehensive analysis but applied to independent case studies at different stations. The addition of COSMO-MUSCAT in our study with respect to the one by Biniotoglou et al. (2015) it is also worthy to point out. The comparison between COSMO-MUSCAT and the other three analyzed models is in our opinion quite interesting, since COSMO-MUSCAT is based in a different philosophy.

#### **Comment:**

**Also, the authors have to further improve the discussion on the skills of the models. The authors calculate the relative bias (what the authors call the Relative Differences); but is this figure good enough to characterize the models? The bias may largely compensate with the layers where under- and overestimations are produced. In other words, a "zero" bias can come from very large absolute errors that compensate. The authors may use the US EPA (1991; 2005) indicators of those statistical figures coming from FAIRMODE initiative in order to have an idea of the ability of the models for reproducing dust must concentration. It would also be desirable to find some information related to the temporal skills: correlation coefficients, variability, etc.**

**Moreover, the authors do not provide any insight on the differences between the models (for instance, why some models indicate dust and some do not) or their skill. This has to be extended in the manuscript.**

#### **Response:**

We agree with the reviewer that additional parameters are needed to better evaluate the model since the use of a single parameter can lead to misleading conclusions. Additional parameters from the documentation suggested by the reviewer have been included in the analysis, namely the root mean square error, the normalized mean bias and the normalized mean standard deviation. The correlation is now also included to evaluate the temporal skills of the models together with the new statistical parameters. Figure13 have been modified including these parameters (see figure below). In order to avoid confusion, some parameters presented in the previous version have now been removed since they do not provide additional information. Discussion has been

modified according to the results observed using the new parameters and extended where necessary.

Additionally, the results section has been reorganized in order to make it easier to follow and try to emphasize the main findings and conclusions inferred from the present study.

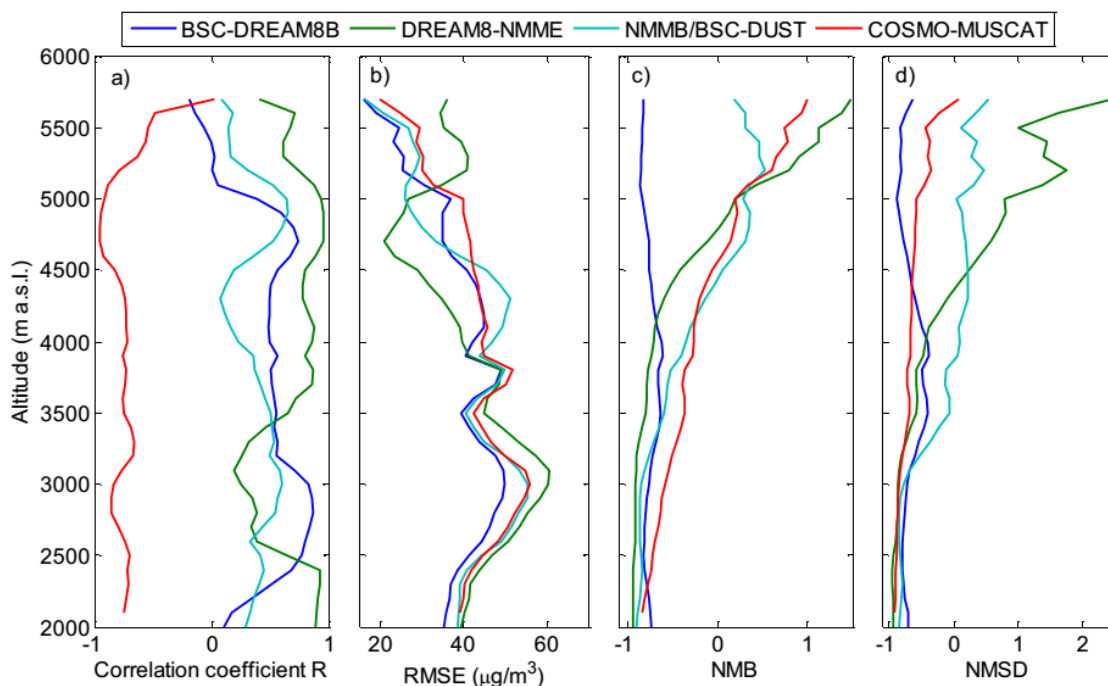


Figure 13. Vertical profiles of the correlation coefficient between LIRIC and the models time series for every altitude level, the root mean square error RMSE, the normalized mean bias NMB and the normalized mean standard deviation NMSD.

#### Other minor comments:

1. I cannot find the reference Gama et al. (2015) in the literature section.

Response:

The reference was not included in the references section. We apologize for the mistake and the reference is now added to the list.

“Gama, C., Tchepel, O., Baldasano, J. M., Basart, S., Ferreira, J., Pio, Cardoso, J., and Borrego, C.: Seasonal patterns of Saharan dust over Cape Verde-a combined approach using observations and modelling. *Tellus B* 2015, 67, 24410, <http://dx.doi.org/10.3402/tellusb.v67.24410>, 2015.”

---

#### Response to Reviewer #3

The authors would like to thank both reviewers for their comments and suggestions, which have helped to improve the quality of the manuscript. Please, find below a detailed response to the reviewer’s comments.

**Comment:**

**The paper it is clearly written and the authors provide an overview on the dust event that mainly affected the western Mediterranean from 9 to 11 July 2012, without adding any new scientific insight on the spatial and temporal evolution of Mediterranean dust events. Therefore, the paper is not appropriate for the ACP journal, to my opinion.**

Response:

The main focus of this paper is on the analysis of the microphysical properties during the ChArMEx campaign in 2012, which has not been presented in previous studies mostly based on the analysis of the aerosol optical properties. We show the utility and the potential of having synergies between lidar and sun/sky radiometer for the vertical profiling of microphysical properties during the day. For example, it is evidenced that the aerosol plume coming from the western Mediterranean area is not the one detected over the Balkan's stations, something that is shown using the synergy between active and passive lidar by applying the LIRIC retrieval algorithm. The study also shows the clear advantage of having additional information such as the data provided by the polarization channels to obtain information about aerosol typing. The simultaneous validation of the different models at different sites together with their temporal evaluation is also one of the main points of the study, since no validation of these characteristics has been presented before.

**Comment:**

**The methodology applied in the paper is commonly used to analyse dust outbreaks and it was also used by Sicard et al., 2015 to characterize the same dust event at the same sites of this study.**

Response:

Sicard et al. (2015) focuses on the optical properties derived from lidar profiles while this paper is focused on exploiting the synergies between active profiling and passive remote sensing to retrieve microphysical properties. In this sense, in this work we present atmospheric profiles of the aerosol concentration, including the splitting between spherical and non-spherical coarse mode particles, something that is really relevant in aerosol typing. Data presented in both studies are complementary of each other.

**Comment:**

**The results referring to Evora should be taken away from the manuscript to my opinion. Note that Fig. 6a of the paper by Sicard et al., (2015) indicates that the Evora lidar signals around 1 km agl were likely affected by the lidar field of view. Note also the sentence at line 225 of the manuscript “ the initial vertical resolution....was established to....100 m”. The aerosol layer of Fig. 6 extends within 200-400 m.**

Response:

Data from Evora are mainly kept in the manuscript to evaluate the performance of the models in cases when no mineral dust is observed. Even though not much information on the microphysical properties can be extracted, we consider data are still valuable and reliable for Evora site. The influence of the lidar incomplete field of view below 1 km mentioned in Sicard et al. (2015) is considered when retrieving the microphysical properties with LIRIC. LIRIC software allows making an interpolation of the data from the lower point of the profile not affected by the incomplete field of view down to the surface. To make the interpolation, LIRIC takes into account the integrated volume concentration provided by the sun photometer for each mode, adjusting the volume concentration profiles to this value. More details can be found in Wagner et al. (2013), Granados-Muñoz et al. (2014) and Chaikovsky et al. (2008; 2016).

The sentence at line 255 refers only to the data used for the model-LIRIC intercomparison. Data presented in figure 6 (figure 4 in the new version of the manuscript) have 15-m vertical resolution. This information has been included in the manuscript.

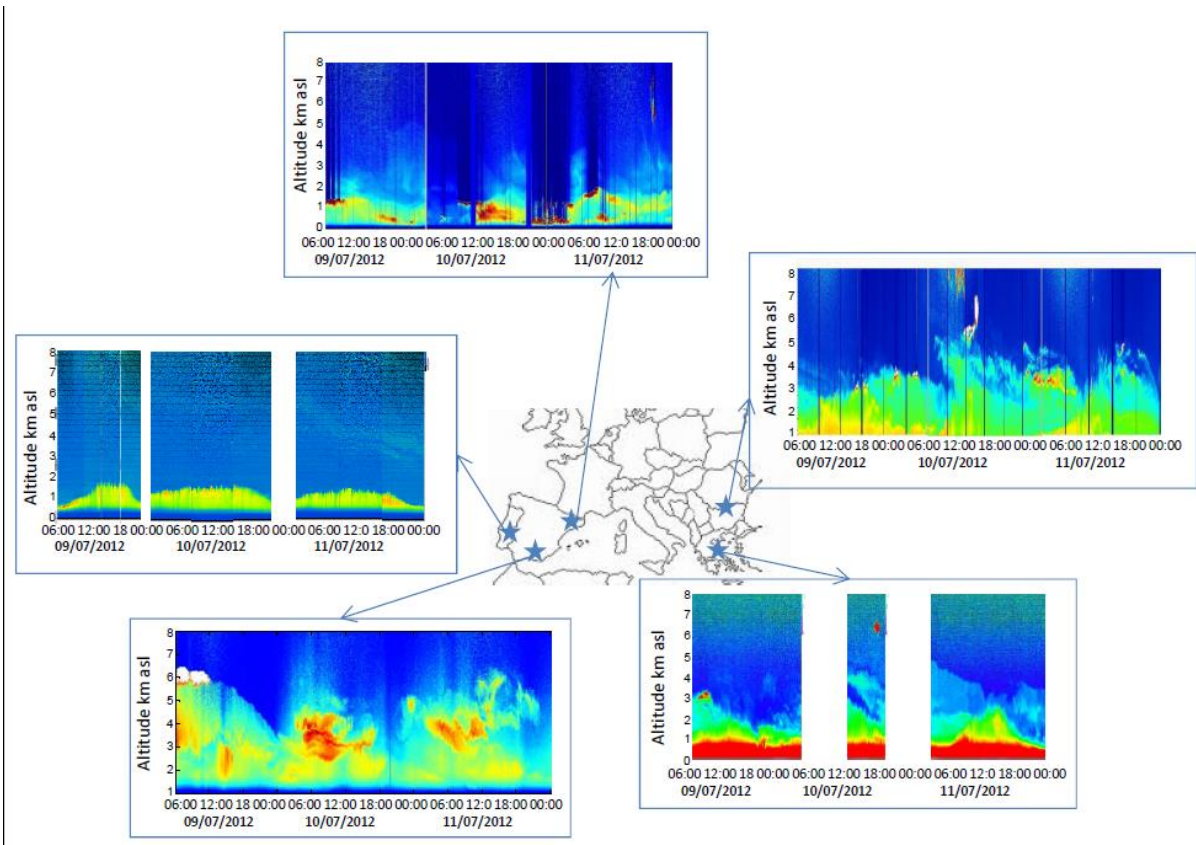
*Line149-150: “From the combination of all this data, volume concentration profiles  $C_v(z_n)$  are obtained for fine and coarse aerosol particles with a vertical resolution of 15 m in our case.”*

**Comment:**

**In addition, I believe that the altitude scale of the RCSs referring to Evora (fig. 5 of the manuscript) is wrong, since it should start at 0 and not at 1 km, as it is clearly shown in Fig. 5a of the paper by Sicard et al., (2015).**

Response:

Scales in Figure 5 were mistaken. We thank the reviewer for pointing it out. Figure 5 (figure 3 in the new version) has been corrected.



**Comment:**

**Lines 529-531:** The sentence “.. the decrease in the fine mode in the coincidence with the increase in the coarse spherical mode could be associated to the aging of the mineral dust particles and aggregation processes” is to my opinion rather speculative.

**Response:**

The sentence has been modified:

Lines 497-502: *“During July 10 in the late afternoon and July 11, a decrease in the fine mode in coincidence with an increase in the coarse spherical mode was observed. The simultaneous decrease of the fine mode and increase of the coarse spherical particles together with the decrease in  $\delta_{532nm}^p$  point out to processes such as mineral dust aging and/or aggregation processes. However, additional analysis would be necessary to confirm this hypothesis.”*

**Comment:**

**I believe that Fig. 6 referring to Granada on 11 July , likely reveals the presence of a dust layer up to about 1.5 km and another dust layer from 3 to about 5.5 km agl. The presence of different dust layers along the aerosol column, as well as the high spatial and temporal variability of the aerosol vertical profile during dust events has been presented and discussed in several papers.**

**Response:**

More detailed information about the dust event at Granada is shown in Figures 9 and 10 (figures 7 and 8 in the new version), whereas figure 6 shows the data at the different stations measured simultaneously in order to see the spatial (both in the vertical and horizontal coordinates) and temporal variability of the microphysical properties during the analyzed event. We would like to emphasize here again that our results are focused on the analysis of the microphysical properties, not the optical properties, which have indeed been analyzed in detail in many previous studies.

Taking into account the comments from both reviewers, part of the manuscript (mainly the results section) has been reorganized and discussion has been extended at some points and reduced where redundant. With this reorganization we intend to highlight the main findings and conclusions inferred from the present study.

---

Marked-up manuscript version:

## PROFILING OF AEROSOL MICROPHYSICAL PROPERTIES AT SEVERAL EARLINET/AERONET SITES DURING JULY 2012 CHARMEX/EMEP CAMPAIGN

M. J. Granados-Muñoz<sup>1,2,\*</sup>, F. Navas-Guzmán<sup>3</sup>, J. L. Guerrero-Rascado<sup>1,2</sup>, J.A. Bravo-Aranda<sup>1,2</sup>, I. Biniotoglou<sup>4</sup>, S. N. Pereira<sup>5</sup>, S. Basart<sup>6</sup>, J.M. Baldasano<sup>6</sup>, L. Belegante<sup>4</sup>, A. Chaikovsky<sup>7</sup>, A. Comerón<sup>8</sup>, G. D'Amico<sup>9</sup>, O. Dubovik<sup>10</sup>, L. Ilic<sup>11</sup>, P. Kokkalis<sup>12</sup>, C. Muñoz-Porcar<sup>8</sup>, S. Nickovic<sup>11,13</sup>, D. Nicolae<sup>4</sup>, F.J. Olmo<sup>1,2</sup>, A. Papayannis<sup>12</sup>, G. Pappalardo<sup>9</sup>, A. Rodríguez-Gómez<sup>8</sup>, K. Schepanski<sup>14</sup>, M. Sicard<sup>8,15</sup>, A. Vukovic<sup>16,13</sup>, U. Wandinger<sup>14</sup>, F. Dulac<sup>17</sup> and L. Alados-Arboledas<sup>1,2</sup>

1 Dpt. Applied Physics, Faculty of Sciences, University of Granada, Fuentenueva s/n, 18071, Granada, Spain

2 Andalusian Institute for Earth System Research (IISTA-CEAMA), Avda. del Mediterráneo s/n, 18006, Granada, Spain

3 Institute of Applied Physics (IAP), University of Bern, Bern, Switzerland

4 National Institute of R&D for Optoelectronics, Magurele, Ilfov, Romania

5 Departamento de Física, ECT, Instituto de Ciências da Terra, IIFA, Universidade de Évora, Portugal.

6 Earth Sciences Department, Barcelona Supercomputing Center-Centro Nacional de Supercomputación, BSC-CNS, Barcelona, Spain

7 Institute of Physics, National Academy of Sciences of Belarus, Minsk, Belarus

8 Dept. of Signal Theory and Communications, Remote Sensing Lab. (RSLab), Universitat Politècnica de Catalunya, Barcelona, Spain

9 Consiglio Nazionale delle Ricerche - Istituto di Metodologie per l'Analisi Ambientale (CNR-IMAA), Potenza, Italy

10 Laboratoire d'Optique Atmosphérique, CNRS Université de Lille 1, Bat P5 Cite scientifique, 59655, Villeneuve d'Ascq Cedex, France

11 Institute of Physics, University of Belgrade, Serbia

12 National Technical University of Athens, Physics Department, Laser Remote Sensing Laboratory, Zografou, Greece

13 South East European Virtual Climate Change Center, Republic Hydrometeorological Service, Belgrade, Serbia

14 Leibniz Institute for Tropospheric Research Leipzig, Germany

15 Ciències i Tecnologies de l'Espai - Centre de Recerca de l'Aeronàutica i de l'Espai / Institut d'Estudis Espacials de Catalunya (CTE-CRAE / IEEC), Universitat Politècnica de Catalunya, Barcelona, Spain

16 Faculty of Agriculture, University of Belgrade, Serbia

17 Laboratoire des Sciences du Climat et de l'Environnement (IPSL-LSCE), CEA-CNRS-UVSQ, CEA Saclay, Gif-sur-Yvette, France

\*Currently at Table Mountain Facility, NASA/Jet Propulsion Laboratory, California Institute of Technology, Wrightwood, California, USA.

Corresponding author: María José Granados Muñoz. Departamento de Física Aplicada, Universidad de Granada, Granada, Spain.

Phone: +34 958 249749

E-mail: mjgranados@ugr.es



## Abstract

The simultaneous analysis of aerosol microphysical properties profiles at different European stations is made in the framework of the ChArMEx/EMEP 2012 field campaign (July 9-11, 2012). During and in support to this campaign, five lidar ground-based stations (Athens, Barcelona, Bucharest, Évora and Granada) performed 72 hours of continuous lidar measurements and collocated and coincident sun-photometer measurements. Therefore it was possible to retrieve volume concentration profiles with the Lidar Radiometer Inversion Code (LIRIC). Results indicated the presence of a mineral dust plume affecting the Western Mediterranean region (mainly Granada station) whereas a different aerosol plume was observed over the Balkans area. LIRIC profiles showed a predominance of coarse spheroid particles above Granada, as expected for mineral dust, and an aerosol plume composed mainly of fine and coarse spherical particles above Athens and Bucharest. Due to the exceptional characteristics of the ChArMEx database, the analysis of the microphysical properties profiles temporal evolution was also possible. An in depth analysis was performed mainly at Granada station because of the availability of continuous lidar measurements and frequent AERONET inversion retrievals. The analysis at Granada was of special interest since the station was affected by mineral dust during the complete analyzed period. LIRIC was found to be a very useful tool for performing continuous monitoring of mineral dust, allowing for the analysis of the dynamics of the dust event in the vertical and temporal coordinates. Results obtained here illustrate the importance of having collocated and simultaneous advanced lidar and sun-photometer measurements in order to characterize the aerosol microphysical properties both in the vertical and temporal coordinates at a regional scale. In addition, this study revealed that the use of the depolarization information as input in LIRIC in the stations of Bucharest, Évora and Granada was crucial for the characterization of the aerosol types and their distribution in the vertical column, whereas in stations lacking of depolarization lidar channels ancillary information was needed. Results obtained were also used for the validation of different mineral dust models. In general, the models better forecast the vertical distribution of the mineral dust than the column integrated mass concentration, which was underestimated in most of the cases.

## 1 1. INTRODUCTION

2 The influence of the atmospheric aerosol particles in the Earth's radiative forcing is still  
3 affected by a large uncertainty, as indicated in the AR5 report from the Intergovernmental  
4 Panel for Climate Change [IPCC, 2013]. During past years, this uncertainty has been  
5 reduced from high to medium with respect to the data in the Fourth Assessment Report  
6 (AR4) of the IPCC, [2007]. However, atmospheric aerosol still contribute to the largest  
7 uncertainty to the total radiative forcing estimate, even though the level of confidence on  
8 the effects of atmospheric aerosols has increased from low and medium to medium and  
9 high (for indirect and direct effect, respectively) [IPCC, 2013].

10 The difficulty in accurately determining atmospheric aerosol properties and their  
11 influence on the Earth's radiative forcing lies in their large spatial and temporal variability.  
12 Ground based (active and passive) remote sensing techniques have proven to be quite  
13 robust and provide accurate results for atmospheric aerosol characterization [e. g. Nakajima  
14 et al., 1996; Dubovik and King, 2000; Mattis et al., 2004; Olmo et al., 2006]. Nonetheless,  
15 they provide information about atmospheric aerosol properties on a local scale. Since  
16 regional analyses are highly important when analyzing the aerosol variability, several  
17 observational networks have been developed. Namely, the lidar network GALION (Global  
18 Atmospheric Watch Aerosol Lidar Observation Network), which includes EARLINET  
19 (European Aerosol Research Lidar Network, [www.earlinet.org](http://www.earlinet.org)) [Bösenberg et al., 2001;  
20 Pappalardo et al., 2014], MPLNET (Micro Pulse Lidar Network) [Welton et al., 2005],  
21 LALINET (Latin American Lidar Network, [www.lalinet.org](http://www.lalinet.org)) [Guerrero-Rascado et al.,  
22 2014] and ADNET (Asian Dust Network) [Shimizu et al., 2004] among others; and the  
23 sun-photometer networks SKYNET (Skyradiometer network) [Takamura and Nakajima,  
24 2004] and AERONET (Aerosol Robotic Network, <http://aeronet.gsfc.nasa.gov/>) [Holben et  
25 al., 1998].

26 In addition to the regional coverage, these networks can provide useful information  
27 on the vertical and temporal coordinates, if adequate measurement protocols are established.  
28 Information on the vertical structure of the aerosol is of high importance, since the  
29 atmospheric aerosol effects can be very different near the surface, within the boundary  
30 layer, and in the free troposphere. Estimates of radiative forcing are sensitive to the vertical  
31 distribution of aerosols [Claquin et al., 1998; Huang et al., 2009; Sicard et al., 2014] and

32 the vertical information is required for accounting the indirect effect [McCormick et al.,  
33 1993; Bréon, 2006]. In addition, atmospheric aerosol can change the vertical profile of  
34 temperature and atmospheric stability, which in turn influences the wind speed profile  
35 within the lower atmosphere [Pérez et al., 2006; Guerrero-Rascado et al., 2009; Choobari et  
36 al., 2014]. Furthermore, continuous and/or regular measurements provided by the networks,  
37 would allow us to analyse the temporal evolution and dynamics of the atmospheric aerosol  
38 particles, which will be very useful not only for accurately determining the radiative  
39 forcing, but also to improve the performance of numerical weather prediction (NWP) [e.g.  
40 Pérez et al., 2006a] and climatological models [Nabat et al., 2014, 2015].

41 Lidar systems are widely used to determine the vertical distribution of aerosols. There are  
42 already many regional studies on the vertical characterization of optical properties based on  
43 lidar systems [e. g. Papayannis et al., 2008]. However, the characterization of the  
44 microphysical properties profiles is still not so straightforward, due to the complexity of the  
45 retrievals. Algorithms designed to combine lidar and sun-photometer measurements have  
46 been developed in order to overcome this difficulty (e.g. Lidar Radiometer Inversion Code,  
47 LIRIC [Chaikovsky et al., 2008; 2012; 2016] and Generalized Aerosol Retrieval from  
48 Radiometer and Lidar Combined data, GARRLIC [Lopatin et al., 2013]. The combination  
49 of simultaneous information about the aerosol vertical structure provided by the lidar  
50 system and the columnar properties provided by the sun photometer has proven to be a  
51 promising synergetic tool for this purpose. LIRIC, which is used in this study, has already  
52 provided interesting results about vertically resolved aerosol microphysical properties for  
53 selected case studies [Tsekeri et al., 2013; Wagner et al., 2013; Granados-Muñoz et al.,  
54 2014; 2015; Papayannis et al., 2014; Biniotoglou et al., 2015]. The increasing number of  
55 stations performing these simultaneous measurements foresees an optimistic future  
56 concerning the increasing spatial coverage.

57 Regional studies in the Mediterranean region are of huge scientific interest since  
58 multiple studies indicate that aerosol radiative forcing over the Mediterranean region is one  
59 of the largest in the world [Lelieveld et al., 2002; IPCC, 2013]. In this context, the  
60 ChArMEx (the Chemistry-Aerosol Mediterranean Experiment, <http://charmex.lsce.ipsl.fr/>)  
61 [Dulac et al., 2014] international project involving several Mediterranean countries aims at  
62 developing and coordinating regional research actions for a scientific assessment of the

63 present and future state of the atmospheric environment in the Mediterranean Basin, and of  
64 its impacts on the regional climate, air quality, and marine biogeochemistry. The ChArMEX  
65 project organized a field campaign between 25 June and 12 July 2012, in order to address  
66 interactions such as long range transport and air quality, and aerosol vertical structure and  
67 sources. The period of the campaign falls within the ACTRIS (Aerosols, Clouds, and Trace  
68 Gases Research Infrastructure Network) summer 2012 campaign (8 June – 17 July, 2012)  
69 that aimed at giving support to both ChArMEX and EMEP (European Monitoring and  
70 Evaluation Programme) [Espen Yttri et al., 2012] field campaigns. Within the ACTRIS  
71 summer 2012 campaign, the European lidar network (EARLINET) [Pappalardo et al.,  
72 2014] performed a controlled exercise of feasibility to demonstrate its potential to perform  
73 operational, coordinated measurements [Sicard et al., 2015]. The exercise consisted of  
74 continuous lidar measurements during a 72-hour period in July 2012 at different European  
75 sites. Most of those lidar data have been successfully assimilated by a regional particulate  
76 air quality model to improve 36-h operational aerosol forecasts both in terms of surface PM  
77 and aerosol optical depth [Wang et al., 2014].

78 Our study takes advantage of those continuous lidar measurements combined with  
79 simultaneous sun-photometer data to perform a characterization of the vertical distribution  
80 of the aerosol microphysical properties at different European stations with LIRIC.  
81 Temporal evolution of the aerosol microphysical properties is also analysed when the  
82 continuity of the inverted data is available. Up to our knowledge, it is the first time that  
83 LIRIC algorithm is applied in a continuous and automated way to retrieve simultaneous and  
84 continuous data acquired at different stations, proving the algorithm capability to provide  
85 reliable microphysical properties information with high spatial and temporal resolution. In  
86 addition, this exceptional aerosol observational database is used for the spatio-temporal  
87 evaluation of different regional mineral dust models

## 88 2. MEASUREMENT STRATEGY

89 During the summer of 2012, an intensive measurement campaign was performed in  
90 the framework of ChArMEX and EMEP in the Mediterranean Basin at twelve ground-based  
91 lidar stations throughout Europe. The main aim of these measurements was to obtain an  
92 experimental vertically-resolved database for investigating aerosol radiative impacts over  
93 the Mediterranean basin using 3-D regional climate models. The extensive lidar database

94 acquired during this campaign combined with AERONET regular measurements represents  
95 a unique opportunity to evaluate the performance of LIRIC microphysical inversion  
96 retrieval during the event in both temporal and spatial (horizontal and vertical) coordinates,  
97 proving the utility of combined measurements and the potential of LIRIC algorithm for  
98 routinary aerosol microphysical properties measurements.

99 The measurement campaign consisted in 72-hours of continuous and simultaneous  
100 lidar measurements performed at twelve European stations, with eleven out of them  
101 participating in ACTRIS/EARLINET [Sicard et al., 2015]. The measurement period started  
102 on July 9 at 06:00 UTC and lasted until July 12, 2012 at 06:00 UTC, in coincidence with a  
103 forecast mineral dust event over the Mediterranean basin according to dust transport  
104 models.

105 LIRIC algorithm requires lidar data at least in 3 different wavelengths and  
106 simultaneous AERONET retrievals in order to obtain the aerosol microphysical properties  
107 profiles. Therefore, to evaluate the performance of LIRIC algorithm and characterize the  
108 distribution and temporal evolution of the aerosol microphysical properties during the  
109 event, only those stations where multiwavelength lidar data at 3 wavelengths and  
110 AERONET data were available for the period July 9-11 were selected. Namely, those  
111 stations were Athens (AT), Barcelona (BA), Bucharest (BU), Évora (EV) and Granada  
112 (GR) (Figure 1). The main characteristics of each station are included in Table 1.

113 [Figure 1]

114 All the five stations are part of both EARLINET and AERONET networks. Thus, these five  
115 stations are equipped with at least a multiwavelength lidar and a sun photometer.  
116 ~~Multiwavelength lidar systems are used in this study to measure vertical profiles of the~~  
117 ~~atmospheric aerosol properties.~~ Lidar systems in all these five stations emit and receive at  
118 least at three different wavelengths (355, 532 and 1064 nm), with the systems in Granada,  
119 Bucharest and Évora including depolarization capabilities at 532 nm (Table 1).  
120 Depolarization information can be used in the retrieval of the aerosol microphysical  
121 properties profiles with LIRIC to distinguish between coarse spherical and coarse spheroid  
122 mode.

123 Stations are also equipped with collocated standard sun photometers CIMEL CE-  
124 318-4, used in the AERONET network. AERONET retrieval algorithm provides  
125 atmospheric aerosol properties integrated in the atmospheric vertical column [Dubovik and  
126 King, 2000; Dubovik et al., 2006]. The automatic tracking sun and sky scanning radiometer  
127 makes sun direct measurements with a  $1.2^\circ$  full field of view every 15 min at different  
128 nominal wavelengths, depending on the station (Table 1). These solar extinction  
129 measurements are used to compute aerosol optical depth ( $\tau_\lambda$ ) at each wavelength except for  
130 the 940 nm channel, which is used to retrieve total column water vapour (or precipitable  
131 water) [Estellés et al., 2006; Pérez-Ramírez et al., 2012]. The estimated uncertainty in  
132 computed  $\tau_\lambda$ , due primarily to calibration uncertainty, is around 0.01–0.02 for field  
133 instruments (which is spectrally dependent, with the larger errors in the UV) [Eck et al.,  
134 1999; Estellés et al., 2006].

135 [Table 1]

### 136 3. METHODOLOGY

#### 137 3.1. RETRIEVAL OF AEROSOL PROPERTIES FROM REMOTE SENSING 138 MEASUREMENTS

139 The analysis of aerosol microphysical properties profiles is performed with LIRIC  
140 algorithm. Details about LIRIC retrieval algorithm and its physical basics can be found in  
141 previous studies [Chaikovsky et al., 2012; 2016; Kokkalis et al., 2013; Wagner et al., 2013;  
142 Granados-Muñoz et al., 2014; 2015; Perrone et al., 2014; Biniotoglou et al., 2015], but a  
143 brief description is included here for completeness. LIRIC provides profiles of atmospheric  
144 aerosol microphysical properties from atmospheric aerosol columnar optical and  
145 microphysical properties retrieved from direct sun and sky radiance measurements from the  
146 sun-photometer using AERONET code (Version 2, Level 1.5) [Dubovik and King, 2000;  
147 Dubovik et al., 2006] and measured lidar elastic backscatter signals at three different  
148 wavelengths (355, 532 and 1064 nm). If available, also the 532-nm cross-polarized signal is  
149 used. Raw lidar data used for this analysis have been prepared accordingly to the  
150 EARLINET Single Calculus Chain (SCC), described in detail in D’Amico et al., [2015].  
151 From the combination of all this data, volume concentration profiles  $C_v(z_n)$  are obtained  
152 for fine and coarse aerosol particles, with a vertical resolution of 15 m in our case. The use

153 of the 532-nm cross-polarized lidar channel allows for distinguishing between spherical and  
154 non-spherical particles within the coarse fraction of the aerosol. The uncertainty in LIRIC  
155 retrievals associated to the input data is not yet well described, but the algorithm has proven  
156 to be very stable and the variations in the output profiles associated to the user-defined  
157 input parameters are below 20% [Granados-Muñoz et al., 2014].

### 158 3.2. MODEL DESCRIPTION AND VALIDATION STRATEGY

159 Models of dust emission, transport and deposition are used as a tool to understand the  
160 various aspects that control distributions and impacts of dust. While global models of the  
161 dust cycle are used to investigate dust at large scales and long-term changes, regional dust  
162 models are the ideal tool to study in detail the processes that influence dust distribution as  
163 well as individual dust events. The analysis of the aerosol microphysical properties with  
164 LIRIC using ChArMEx comprehensive database was used here for the evaluation of a set  
165 of 4 regional mineral dust models. This model evaluation was performed for both the  
166 vertical and horizontal coordinates and the temporal evolution.

167 Firstly, the spatial distribution of the mineral dust was examined by using the  
168 experimental data from the five EARLINET/AERONET sites considered in the present  
169 study. Dust optical depth (at 550nm) provided by four different regional mineral dust  
170 models (BSC-DREAM8b, NMMB/BSC-Dust, DREAM8-NMME and the regional version  
171 of COSMO-MUSCAT) was used at this stage. Experimental data were used here just to  
172 corroborate the presence or non-presence of mineral dust at the different regions and  
173 periods indicated by the models.

174 BSC-DREAM8b and DREAM8-NMME models are based on the Dust Regional  
175 Atmospheric Model (DREAM), originally developed by Nickovic et al., [2001]. The main  
176 feature of the updated version of the model, BSC-DREAM8b (version 2), include an 8-bins  
177 size distribution within the 0.1–10  $\mu\text{m}$  radius range according to Tegen and Lacis [1996],  
178 radiative feedbacks [Pérez et al., 2006a,b] and upgrades in its source mask [Basart et al.,  
179 2012]. BSC-DREAM8b model provides daily dust forecasts at Barcelona Supercomputing  
180 Center–Centro Nacional de Supercomputación (BSC-CNS,  
181 <http://www.bsc.es/projects/earthscience/BSC-DREAM/>). The model has been extensively  
182 evaluated against observations [see, e.g. Basart et al. 2012b]. Recently, the DREAM8-

183 NMME model [Vukovic et al, 2014], driven by the NCEP Nonhydrostatic Mesoscale  
184 Model on E-grid [Janjic et al., 2001], provides daily dust forecasts available at the South  
185 East European Virtual Climate Change Center (SEEVCCC; <http://www.seevccc.rs/>).

186 NMMB/BSC-Dust model [Pérez et al., 2011; Haustein et al., 2012] is a regional to  
187 global dust forecast operational system developed and maintained at BSC-CNS. It is an  
188 online multi-scale atmospheric dust model designed and developed at BSC-CNS in  
189 collaboration with NOAA-NCEP, NASA Goddard Institute for Space Studies and the  
190 International Research Institute for Climate and Society (IRI). NMMB/BSC-Dust model  
191 includes a physically based dust emission scheme, which explicitly takes into account  
192 saltation and sandblasting processes. It includes an 8-bin size distribution and radiative  
193 interactions. NMMB/BSC-Dust model has been evaluated at regional and global scales  
194 [Pérez et al. 2011; Haustein et al. 2012; Gama et al., 2015].

195 BSC-DREAM8b, NMMB/BSC-DDUST and DREAM8-NMME models are  
196 participating in the World Meteorological Organization Sand and Dust Storm Warning  
197 Advisory and Assessment System (WMO SDS-WAS) Northern Africa-Middle East-Europe  
198 (NAMEE) Regional Center (<http://sds-was.aemet.es/>). Additionally, NMMB/BSC-Dust is  
199 the model that provides operational dust forecast in the first Regional Specialized  
200 Meteorological Center with activity specialization on Atmospheric Sand and Dust Forecast,  
201 the Barcelona Dust Forecast Center (BDFC; <http://dust.aemet.es/>).

202 On the other hand, COSMO-MUSCAT is an online coupled model system based on a  
203 different philosophy: COSMO is a non-hydrostatic and compressible meteorological model  
204 which solves the governing equations on the basis of a terrain-following grid [Schättler et  
205 al., 2008; Baldauf et al., 2011], whereas MUSCAT is a chemistry transport model that  
206 treats the atmospheric transport as well as chemical transformations for several gas phase  
207 species and particle populations using COSMO output data [Knoth and Wolke, 1998;  
208 Wolke et al. 2012]. More details about COSMO-MUSCAT model can be found elsewhere  
209 [Schepanski et al., 2007, 2009; Heinold et al., 2009; Laurent et al., 2010; Tegen et al.,  
210 2013].

211 The spatial resolution, domain size, initial and boundary conditions, differ, in  
212 addition to the different physical parameterizations implemented in the models. Details on



213 the individual mineral dust models and their respective model configurations evaluated here  
214 are summarized in Table 2.

215 [Table 2]

216 In a further step, modelled mineral dust mass concentration profiles were compared  
217 with LIRIC output profiles in order to evaluate the model performance on the vertical  
218 coordinate. The temporal evolution of the modelled vertical profiles was evaluated in more  
219 detail only at Granada, which was the station most affected by the dust outbreak during the  
220 analysed period and thus provided a more extensive database. Since LIRIC provides  
221 volume concentration profiles, a conversion factor was needed to obtain mass  
222 concentration. This conversion factor was the density of the aerosol particles, namely  $2.65$   
223  $\text{g}\cdot\text{cm}^{-3}$  for the coarse mode (1-10  $\mu\text{m}$ ) and  $2.5 \text{ g}\cdot\text{cm}^{-3}$  (0.1-1  $\mu\text{m}$ ) for the fine mode [Pérez et  
224 al., 2006a,b]. In addition, the initial vertical resolution of the different models and LIRIC  
225 was established to a common values of 100 m, in order to obtain a compromise between the  
226 loss of information from LIRIC and from the different models, following a similar  
227 procedure to that in Binietoglou et al., [2015].

228 After this processing, mineral dust mass concentration profiles provided by BSC-  
229 DREAM8b, NMMB/BSC-DUST, DREAM8-NMME and COSMO-MUSCAT models were  
230 evaluated against LIRIC results in those cases when mineral dust was detected. For the  
231 comparison, the fine mode was assumed to be fine mineral dust since it is not possible to  
232 distinguish which part of the fine mode corresponds to dust or non-dust particles with  
233 LIRIC. This assumption may cause an overestimation of the mineral dust concentration that  
234 becomes more important in those cases with high concentrations of the fine mode (which  
235 was not the case in our study). Alternative methods, such as POLIPHON (Polarization-lidar  
236 photometer networking) method, could be applied to overcome this difficulty [Mamouri  
237 and Ansmann, 2014], but this is out of the scope of our study.

238 In our study, model output profiles were retrieved every 3 hours and compared to  
239 LIRIC retrievals during the three analyzed days. Only daytime data are presented here  
240 (from 06:00 to 18:00 UTC) because of the limitations of LIRIC retrieval during night-time.  
241 Due to the difficulties of the models to correctly represent the convective processes  
242 occurring within the planetary boundary layer and PBL-free troposphere interactions and

243 the photochemical reactions producing secondary aerosols at the considered resolution, the  
 244 lowermost part of LIRIC profiles (affected by these processes) was not considered in the  
 245 comparison presented here. Only data between 2000 m asl, which is the mean value of the  
 246 PBL height during summer at Granada [Granados-Muñoz et al., 2012], and the highest  
 247 value (up to between 5 and 6 km) provided by LIRIC were included in the comparisons.

248 In order to quantify the model agreement with the total dust load observed in the  
 249 profiles, the integrated dust mass concentration from the different profiles was obtained by  
 250 integrating the profiles between 2 km asl and the highest altitude value provided by LIRIC  
 251 profiles.

252 The altitude of the center of mass of the dust column ( $C_m$ ) was also calculated  
 253 according to Equation 1, where  $z_{min}$  and  $z_{max}$  are 2 and the highest altitude value provided  
 254 by LIRIC respectively:

255

$$256 \quad C_m = \frac{\int_{z_{min}}^{z_{max}} z_n C_{mass}(z_n) dz_n}{\int_{z_{min}}^{z_{max}} C_{mass}(z_n) dz_n} \quad (1)$$

257 Additional parameters used in the comparison between LIRIC and the model dust  
 258 mass concentration profiles are the root mean square error (RMSE), the correlation  
 259 coefficient (R), the normalized mean bias (NMB) and the normalized mean standard  
 260 deviation (NMSD), defined in equations 2 to 6:

$$261 \quad RMSE = \sqrt{\frac{1}{n} \sum_n (C_{mass}^{LIRIC}(z_n) - C_{mass}^{model}(z_n))^2} \quad (2)$$

$$262 \quad R = \frac{\sum_n (C_{mass}^{model}(z_n) - \overline{C_{mass}^{model}})(C_{mass}^{LIRIC}(z_n) - \overline{C_{mass}^{LIRIC}})}{\sqrt{\sum_n (C_{mass}^{model}(z_n) - \overline{C_{mass}^{model}})^2} \sqrt{\sum_n (C_{mass}^{LIRIC}(z_n) - \overline{C_{mass}^{LIRIC}})^2}} \quad (3)$$

$$263 \quad NMB = \frac{\overline{C_{mass}^{model}} - \overline{C_{mass}^{LIRIC}}}{\overline{C_{mass}^{LIRIC}}} \quad (4)$$

$$264 \quad NMSD = \frac{\sigma_{model} - \sigma_{LIRIC}}{\sigma_{LIRIC}} \quad (5)$$

265 where n is the number of height levels;  $C_{mass}(z_n)$  is the dust mass concentration at  
 266 each height level  $z_n$ , either for LIRIC or the models;  $\overline{C_{mass}}$  are mean values; and  
 267  $\sigma$  indicates the standard deviation.

268 A detailed comparison of BSC-DREAM8b, NMMB/BSC-DUST, DREAM8-NMME  
269 (three out of the four models presented here) dust mass concentration profiles with LIRIC  
270 results was performed in Binietoglou et al. [2015] using additional stations and selected  
271 case studies for the period 2011-2013. However, due to the characteristics of ChArMEx  
272 database this study goes a step further. Up to our knowledge, it is the first time that the  
273 different models are evaluated at different stations using simultaneous data, thus providing  
274 information about the horizontal coordinate, following the evolution of a regional event.  
275 Additionally, a validation of the mass concentration profiles temporal evolution of a  
276 specific mineral dust event is presented for the first time.

277

## 278 4. RESULTS

279

280 During the 72-hour intensive measurement period, information from different models,  
281 platforms and instrumentation was available. A detailed characterization of the situation  
282 above the Mediterranean Basin during the campaign focused on aerosol microphysical  
283 properties using the different resources available is presented in the subsection 4.1.,  
284 followed by the models evaluation in subsection 4.2.

### 285 4.1. SPATIAL-TEMPORAL CHARACTERIZATION OF AEROSOL 286 MICROPHYSICAL PROPERTIES DURING CHARMEX/EMEP 2012

#### 287 4.1.1. Ground-based column-integrated measurements

288 Column-integrated properties retrieve from the AERONET sun-photometer are  
289 presented in Figure 2. Figure 2a and b shows the time series of the  $\tau_{440\text{nm}}$  and AE(440-  
290 880nm) for the selected 5 stations during the analysed period and mean values for each day  
291 and station are indicated in Table 3.

292 According to these data, the lowest values of  $\tau_{440\text{nm}}$  were measured at Évora station  
293 during the whole period, with values below 0.18. The AE(440-880nm) was close to one,  
294 except in the early morning and late evening, when it decreased down to ~0.5. These  
295 values, together with the columnar volume size distributions observed in Figure 2c  
296 indicates a very low aerosol load, mostly related to aerosol from local sources, and no

297 impact of the North African aerosol plume forecast to arrive at the Iberian Peninsula. A  
298 decrease of  $\tau_{440\text{nm}}$  value with time was observed at Granada station, with maximum values  
299 reaching up to 0.40 on July 9 around 16:00 UTC. During July 10 and 11,  $\tau_{440\text{nm}}$  values were  
300 between 0.10 and 0.20, except for the late afternoon of July 10 from 17:00 UTC, when the  
301 aerosol load decreased and  $\tau_{440\text{nm}}$  below 0.10 were observed. On the contrary, values of the  
302 AE(440-870 nm) were increasing from 0.3 on July 9 up to 0.7 on July 11, with maximum  
303 values on the late evening on July 10 ( AE(440-870 nm) >1). It is worthy to note that the  
304 AE(440-870nm) was below 0.5 during the whole period except for the late afternoon on  
305 July 10, in coincidence with the decrease in  $\tau_{440\text{nm}}$ , indicating a clear predominance of  
306 coarse particles [e. g. Pérez et al., 2006a; Basart et al., 2009; Valenzuela et al., 2014]. The  
307 columnar volume size distributions for the different days agreed with these data. Data from  
308 July 9 show a very large coarse mode and a small contribution of fine particles. The  
309 contribution of fine particles was almost constant during the three days, whereas the coarse  
310 mode was decreasing with time. There was a predominance of the coarse mode during the  
311 whole period, with maximum values of  $0.13 \mu\text{m}^3/\mu\text{m}^2$  during the first day. All these data are  
312 usually related to the presence of mineral dust in the station and the temporal evolution of  
313 the analyzed properties clearly suggest a decrease of the mineral dust event intensity  
314 throughout the analysed period and a possible mixing or aging of the mineral dust. At  
315 Barcelona station no AERONET data were available on July 9. During July 10 and 11,  
316  $\tau_{440\text{nm}}$  values were relatively high and quite constant (around 0.30) and the AE(440-870nm)  
317 values were larger than 1.5, indicating a strong contribution of fine aerosol particles. In the  
318 columnar volume size distributions, similar values for the fine and coarse mode were  
319 observed on the July 10, but larger values of the fine mode were obtained on July 11.  
320 Therefore, it can be inferred from these data that the impact of the North African aerosol  
321 plume was almost negligible at this station.

322 In Athens and Bucharest the aerosol plume presented very different characteristics to those  
323 observed on the Western region. **Error! Reference source not found.**In this region, large  
324  $\tau_{440\text{nm}}$  values (>0.35) and large values of the AE(440-870 nm) suggested a situation with  
325 high aerosol load mainly composed of fine particles. At Athens both  $\tau_{440\text{nm}}$  and AE(440-870  
326 nm) values were very constant during the three analysed days, except for a slight decrease  
327 of the AE(440-870nm) on July 11 (from ~1.70 to ~1.30). This is in agreement with the

328 columnar volume size distributions (Figure 3c), where a slight increase of the coarse mode  
329 was observed on July 11 when compared to July 9 and 10. In the case of Bucharest,  $\tau_{440\text{nm}}$   
330 was almost constant on July 9 and 10 (around 0.37), but increased on July 11 (over 0.60).  
331 The AE(440-870nm) was almost constant around 1.10 during the three days, indicating a  
332 balanced presence of coarse and fine particles despite the increase in the aerosol load  
333 during July 11. The columnar volume size distributions were very similar to those of  
334 Athens on July 9 and 10, but larger presence of fine particles was observed here on July 11.  
335 According to these sun-photometer data, the aerosol plume over this region was not  
336 composed of mineral dust particles, even though low concentrations of mineral dust might  
337 have been advected over Athens on July 11.

338 [Table 3]

339 [Figure 2]

340

341 4.1.2. Aerosol vertical distribution

342 [Figure 3]

343 Figure 3 shows the time series of the lidar range-corrected signal (RCS) in arbitrary  
344 units at 532 nm (at 1064 nm in Athens) for the 72-hour period at the different stations.  
345 From these plots, it is clearly observed that at Barcelona and Évora the aerosol load was  
346 mainly confined within the planetary boundary layer and the time series reveal the  
347 evolution of the planetary boundary layer height, even though at Barcelona some aerosol  
348 layers are observed in the free troposphere. Therefore, it is expected that most of the  
349 aerosol particles are from local origin. However, at the rest of the stations a more complex  
350 vertical structure was observed and the presence of lofted aerosol layer reaching up to 6 km  
351 asl at some periods indicated the advection of different aerosol types.

352 [Figure 4]

353 The aerosol microphysical properties profiles retrieved with LIRIC for different  
354 periods at the different stations are shown in Figure 4. Namely, the volume concentration  
355 profiles of the total coarse mode and the fine mode were retrieved at Barcelona and Athens,  
356 whereas the volume concentration profiles of fine, coarse spherical and coarse spheroid

357 mode were retrieved at Évora, Bucharest and Granada because of the availability of  
358 depolarization information.

359 At Évora it was clearly observed that the aerosol was located below 1000 m asl,  
360 within the planetary boundary layer, and concentrations were very low, ranging from 25 to  
361  $46 \mu\text{m}^3 \cdot \text{cm}^{-3}$ . No advected aerosol layers were observed for the analysed period.

362 At Granada a clear predominance of coarse spheroid particles reaching altitudes  
363 around 6000 m asl was observed on July 9, related to the mineral dust event. A small  
364 contribution of fine particles was also observed during the three days. Values of the volume  
365 concentration (below  $50 \mu\text{m}^3 \cdot \text{cm}^{-3}$  for the total concentration) indicate a medium intensity  
366 dust event, which was considerably decreasing with time. Concentration values around 30  
367  $\mu\text{m}^3 \cdot \text{cm}^{-3}$  on July 9 for the coarse spheroid mode went down to values below  $20 \mu\text{m}^3 \cdot \text{cm}^{-3}$ .  
368 The altitude of the mineral dust layers was also decreasing from 6000 to 4000 m asl for the  
369 highest layers.

370 At Barcelona site, an aerosol layer dominated by fine particles with a slight presence  
371 of coarse particles was observed between 2000 and 4000 m asl on July 11, being these  
372 coarse particles possibly related to a faint presence of mineral dust. The 5-day backward  
373 trajectories analysis performed with HYSPLIT model [Draxler and Rolph, 2003] (not  
374 shown) indicates that air masses arriving at this altitude came from the North of Africa  
375 through the Iberian Peninsula. This information together with previous studies [e.g Wang et  
376 al., 2014], suggest that the mineral dust plume was moving from the North of Africa  
377 towards the Northeast, being detected at Granada and later on at Barcelona. However, the  
378 possibility of these coarse particles being linked to the presence of biomass burning from  
379 the Eastern Iberian Peninsula (see Figure 5) cannot be dismissed. Depolarization  
380 information would be crucial here to discriminate the origin of the aerosol particles arriving  
381 at this height above Barcelona and would provide very valuable information for the aerosol  
382 typing at the station.

383 At Athens station the aerosol reached up to 5000 m asl and total concentration values  
384 of up to  $55 \mu\text{m}^3 \cdot \text{cm}^{-3}$  in the free troposphere. The coarse mode was located below 2000 m  
385 asl, whereas a predominance of fine particles was observed at higher altitudes. The top of  
386 the aerosol layer was increasing with time from 3800 to almost 5000 m asl. This temporal

387 evolution of the microphysical properties is coherent with the optical properties shown in  
388 Sicard et al., [2015] for the same period. It is worthy to point out that on July 11, coarse  
389 particles were detected between 3000 and 4800 m asl at this station, probably related to the  
390 arrival of mineral dust as indicated by the column-integrated values. Backward trajectories  
391 analysis with HYSPLIT (not shown) revealed a change in the trajectory of the air masses  
392 arriving at 3500 m asl, coming from Northern Africa, which would explain the presence of  
393 mineral dust on July 11. However, according to the trajectories and the different  
394 characteristics, the mineral dust observed at Athens corresponds to a different plume than  
395 the one observed above Granada and faintly above Barcelona.

396 At Bucharest, similar volume concentration of fine and coarse particles was observed  
397 on July 9 and 10, reaching total volume concentration values around  $35 \mu\text{m}^3\text{cm}^{-3}$ . The  
398 observed coarse particles were spherical according to LIRIC; therefore the presence of  
399 mineral dust at this region can be totally neglected. On July 11 a strong increase of the fine  
400 mode volume concentration was observed between 2500 and 5000 m asl, with values  
401 reaching up to  $55 \mu\text{m}^3\text{cm}^{-3}$ , suggesting the advection of an aerosol plume dominated by  
402 fine particles at this altitude. Again, this is in agreement with the optical properties  
403 presented in Sicard et al. [2015], where a larger spectral dependence (related to fine  
404 particles) is observed at Bucharest station in the height range between 3 and 4 km asl. As  
405 suggested in the study by Sicard et al. [2015] this large spectral dependence of the  
406 backscatter coefficient could be originated by the presence of fine particles related to the  
407 advection of smoke. The combined information provided by backward trajectories analysis  
408 and MODIS FIRMS comes to confirm the presence of active fires along the air masses  
409 paths arriving at Bucharest on July 11 (Figure 5).

410

411

[Figure 5]

412

413 The use of the depolarization information as input in LIRIC in the stations of  
414 Bucharest, Évora and Granada provided additional information which is very valuable for  
415 aerosol typing. In the cases of Bucharest and Granada, this information turned out to be  
416 very useful for the characterization of the aerosol types and their distribution in the vertical

417 coordinates. The differences in the aerosol type were already evidenced in the columnar  
418 volume size distributions retrieved by AERONET code ([Figure 2](#)), and here LIRIC  
419 confirmed that these two stations presented really different situations. The volume  
420 concentration profiles retrieved with LIRIC indicated a predominance of the spheroid mode  
421 in Granada and a predominance of spherical particles in Bucharest, highlighting very  
422 different aerosol composition in the coarse mode. However, at stations such as Barcelona or  
423 Athens where lidar depolarization was not measured, ancillary information, e.g. backward  
424 trajectories or sun-photometer-derived optical properties, was needed to discriminate if the  
425 coarse mode was related to non-spherical particles, usually associated to mineral dust, or to  
426 spherical particles, mostly present in cases of anthropogenic pollution or aged smoke.  
427 Therefore, here we have a clear example of the importance and the potential of the  
428 depolarization measurements in the vertical characterization of the aerosol particles and for  
429 aerosol typing.

#### 430 4.1.3. Temporal evolution of the aerosol microphysical properties profiles

431 The continuous analysis of the aerosol microphysical properties profiles during the  
432 three days provided very valuable information about the dynamics of the aerosol layers and  
433 revealed LIRIC potential to retrieve information with high temporal resolution. Because of  
434 the uninterrupted lidar measurements at Granada from 12:00 UTC on July 9 2012 to 00:00  
435 UTC on July 12 and the frequent AERONET retrievals due to good weather conditions a  
436 more detailed analysis was performed at this station. A total of 60 different LIRIC  
437 retrievals were performed based on 60 lidar datasets and 21 AERONET inversion  
438 products. The retrieval of microphysical properties was performed using 30-min averaged  
439 lidar data (in order to reduce noise on the lidar profiles) and the closest in time AERONET  
440 retrieval, considering only those data with time differences lower than three hours.

441 Besides, Granada station was affected by a mineral dust event during the whole  
442 period as already shown in previous sections. This fact is of special interest since the  
443 retrieval of the mineral dust microphysical is not so straightforward and they are not so well  
444 characterized. Up to our knowledge not many comprehensive studies on dust microphysical  
445 properties vertical profiles have been performed [Tsekeri et al., 2013; Wagner et al., 2013;  
446 Granados-Muñoz et al., 2014; Noh, 2014] because of the difficulty of the retrievals due to  
447 different factors, e. g. the high temporal variation and non-uniform distribution of dust



448 aerosol concentration around the globe [Sokolik and Toon, 1999; Formenti et al., 2011],  
449 mineral dust highly irregular shape and the chemical and physical transformations dust  
450 suffers during its transport [Sokolik and Toon, 1999; Chen and Penner, 2005; Formenti et  
451 al., 2011].

452 The dust outbreak analysed here started over Granada station on July 7 in 2012 as  
453 indicated by sun-photometer data and the model forecast from previous days (not shown).  
454 Thus, it was already well developed when the intensive measurement period started. The 5-  
455 day backward trajectories analysis performed with HYSPLIT model indicated that the air  
456 masses arriving at Granada on July 9 and 11 came from Africa passing by the North  
457 African coast above 2500 m asl and from the North Atlantic Ocean through South-western  
458 Iberian Peninsula below this altitude (Figure 6). On July 10 the air masses came from the  
459 central part of the Sahara desert through the North African coast for heights above 5000 m  
460 asl, from the Atlantic Ocean going along the coast of Africa between 2500 and 5000 m asl  
461 and from the North Atlantic Ocean overpassing the South-western Iberian Peninsula below  
462 2500 m asl.

463  
464  
465

[Figure 6]

466 Figure 7 shows the time series of the volume concentration profiles retrieved with  
467 LIRIC. It is clearly observed that the dust event was decreasing its intensity along the  
468 whole study period with the largest aerosol concentrations for the coarse spheroid mode  
469 retrieved on July 9 ( $\sim 35 \mu\text{m}^3/\text{cm}^3$ ) and the lowest concentrations on July 11 ( $\sim 15 \mu\text{m}^3/\text{cm}^3$ ),  
470 in agreement with AERONET data. Maximum values of total volume concentration were  
471 around  $60 \mu\text{m}^3\text{cm}^{-3}$  on July 9. There was a strong predominance of the coarse spheroid  
472 mode during the whole period with maximum values on July 9 in the afternoon, reaching  
473 values up to  $55 \mu\text{m}^3\text{cm}^{-3}$ . Some fine particles were also observed, with larger volume  
474 concentrations during the first day ( $\sim 10 \mu\text{m}^3\text{cm}^{-3}$ ). For this first day of measurements, fine  
475 particles reached altitudes around 6000 m asl, whereas on July 10 and 11 larger volume  
476 concentration values were confined to the lowermost region from surface up to 3 km asl.  
477 The presence of this fine mode in the upper layers might be related to the advection of  
478 anthropogenic pollutants coming from Moroccan industrial activity in the North of Africa

479 mixed with the mineral dust as reported in previous studies [Basart et al., 2009; Rodríguez  
480 et al., 2011; Valenzuela et al., 2012; Lyamani et al., 2014; Valenzuela et al., 2014]. Figure  
481 6b reveals that air masses overpassed North African industrial areas before reaching  
482 Granada. However, it is also well known that mineral dust emissions produce a  
483 submicronic size mode [e.g. Gomes et al., 1990; Alfaro and Gomes, 2001]. Depolarization  
484 lidar observations over the Mediterranean have illustrated that irregularly shaped fine dust  
485 particles significantly contribute to aerosol extinction over the boundary layer during dust  
486 transport events [Mamouri and Ansmann, 2014]. A more detailed analysis with additional  
487 data (e.g. chemical components measurements, single scattering albedo profiles) would be  
488 needed in order to come to a quantitative attribution of soil dust and anthropogenic particles  
489 to the fine mode.

490 The contribution of the fine mode in the lowermost part may be due mainly to  
491 anthropogenic sources of local origin. From July 11 around 12:00 UTC up to the end of the  
492 study period, an increase in the coarse spherical mode concentration was observed. This  
493 increase of the coarse spherical mode was associated with a decrease of the particle linear  
494 depolarization profiles  $\delta_{532nm}^p$  obtained from the lidar data according to [Bravo-Aranda et  
495 al., 2013] as shown in Figure 8. On July 9 the values of  $\delta_{532nm}^p$  were around 0.30 in the  
496 layer between 3 and 5 km asl. These values are representative of pure Saharan dust  
497 [Freudenthaler et al., 2009]. However, they decreased down to 0.25 during the following  
498 days, indicating either a possible mixing of dust particles with anthropogenic aerosols or  
499 aging processes affecting the mineral dust. During July 10 in the late afternoon and July 11,  
500 a decrease in the fine mode in coincidence with an increase in the coarse spherical mode  
501 was observed. The simultaneous decrease of the fine mode and increase of the coarse  
502 spherical particles together with the decrease in  $\delta_{532nm}^p$  point out to processes such as  
503 mineral dust aging and/or aggregation processes. However, additional analysis would be  
504 necessary to confirm this hypothesis.

505 According to  $\delta_{532nm}^p$  profiles, a mineral dust layer was clearly located above 2500 m  
506 asl or even at higher altitudes depending on the analysed period (see Figure 10). Below this  
507 altitude, values were lower indicating a mixing of the mineral dust with anthropogenic  
508 particles from local origin. In the case of LIRIC, these vertical structures were not so

509 clearly defined and a more homogeneous structure was detected. Values of the fine and  
510 coarse mode volume concentration presented very low variations with height when  
511 compared to  $\delta_{532nm}^p$  profiles. This vertical homogeneity is related to the assumption of  
512 height independency of properties such as the refractive index, size distribution of the  
513 modes or the sphericity, which according to the results presented in previous studies  
514 [Wagner et al., 2013; Granados-Muñoz et al., 2014], is an issue that needs to be carefully  
515 considered in the analysis of the results retrieved with LIRIC algorithm.

516 [Figure 7]

517 [Figure 8]

518 Despite the limitations in the use of LIRIC, the analysis presented here shows that LIRIC  
519 can reliably provide microphysical properties profiles with high vertical and temporal  
520 resolution even in cases of mineral dust. LIRIC algorithm can be a useful tool to detect  
521 changes in the aerosol composition possibly associated to processes affecting the mineral  
522 dust particles such as aging or nucleation, even though additional information is needed for  
523 more in-depth analysis.

#### 524 4.2. EVALUATION OF THE MINERAL DUST MODELS

525 In order to obtain a general overview of the dust horizontal extension, Figure 9 shows  
526 the standard aerosol optical depth product retrieved using the dark-target approach from  
527 MODIS/Terra [Remer et al., 2005 and references therein] and the AERUS-GEO from  
528 MSG/SEVIRI [Carrer et al., 2014] for the three analysed days (9-11 July 2012).

529 [Figure 9]

530 Satellite data evidence the presence of an aerosol plume extending from the North  
531 African coast towards the East with higher aerosol load, as  $\tau_{\lambda}$  values from MODIS sensor  
532 indicate, mainly affecting the South-East of the Iberian Peninsula and the South of Italy  
533 (Figure 9). As indicated by the data presented in the previous section, this plume  
534 corresponds to the mineral dust event, whereas a different plume is observed above the  
535 Balkans area. The pathways of the aerosol plumes suggested by satellite data are in  
536 agreement with both the meteorological analyses of ECMWF and HYSPLIT air mass  
537 trajectories based on GDAS analysed meteorological fields at 2 km a.g.l. presented in the

538 study by Wang et al., [2014]. The air masses were moving from Spain and Portugal to the  
539 East whereas in the Balkans region they were moving southwards.

540 [Figure 10]

541  $\tau_{550\text{nm}}$  data simulated by BSC-DREAM8b, DREAM8-NMME NMMB/BSC-Dust and  
542 COSMO-MUSCAT are shown in Figure 10. In general, when comparing to the satellite  
543 data in Figure 9, the aerosol plume located above the Balkans region is not captured by the  
544 models. This is not surprising, since it is not composed of mineral dust particles, as  
545 indicated by our aerosol volume concentration profiles, shown in the previous section and  
546 suggested in previous studies [e.g. Sicard et al., 2015]. The different models correctly  
547 forecast the dust plume leaving the North of Africa and moving towards the East and the  
548 dust plume reaching Athens, as also indicated by satellite data. However, the decrease in  
549  $\tau_{550\text{nm}}$  values with time observed with satellite data and in LIRIC profiles is not well  
550 captured by any of the different models. Regarding the extension of the dust event, in  
551 general it is better captured by BSC-DREAM8b and NMMB/BSC-Dust, whereas COSMO-  
552 MUSCAT and DREAM8-NMME tend to overestimate the mineral dust horizontal  
553 extension when compared to the satellite data.

554 Focusing on the five stations analyzed in this study, the models showed that Granada  
555 station was affected by the mineral dust outbreak during the whole analyzed period, in  
556 agreement with the analyzed data. No presence of mineral dust was forecast above Évora as  
557 expected from the measurements, except for COSMO-MUSCAT, which predicted fair low  
558 values of dust  $\tau_{550\text{nm}}$  above the station. BSC-DREAM8b, DREAM8-NMME and  
559 NMMB/BSC-Dust indicated no presence of dust above Barcelona, even though it was  
560 located close to the edge according to BSC-DREAM8b. As in the case of Évora, almost  
561 negligible values were forecast above the station by COSMO-MUSCAT. This would be in  
562 agreement with the previous data except for the possible dust layer observed on July 11.

563 In the Eastern region, the station of Athens was affected by mineral dust during the three  
564 days according to DREAM8-NMME model and COSMO-MUSCAT, only on July 10  
565 according to NMMB/BSC-Dust and on July 10 and 11 according to BSC-DREAM8b. As  
566 indicated by the analysis in the previous section, mineral dust was observed only on July 11  
567 and the models seem to not completely capture the event at Athens. However, in this case

568 the situation is quite more complex than in the western stations. Athens is located at the  
569 edge of the mineral dust plume during the three analyzed days. Slight changes in the  
570 horizontal distribution of the dust related to the models uncertainty and the relatively coarse  
571 horizontal resolution may highly influence the results. In the case of Bucharest, BSC-  
572 DREAM8b, DREAM8-NMME and NNMB/BSC-DUST foresaw no influence of the  
573 mineral dust. Conversely, COSMO-MUSCAT forecast mineral dust during the three days,  
574 with larger loads on July 10 and 11, overestimating the extension of the mineral dust  
575 plumes as previously stated.

576 Due to the relatively coarse horizontal resolution of the model data presented in  
577 Figure 10 compared to the single-site measurements at the five analyzed stations, it is  
578 worthy to evaluate in more detail the mineral dust mass concentration profiles provided by  
579 the models at the specific locations of our interest. To perform this evaluation, mineral dust  
580 mass concentration profiles provided by the BSC-DREAM8b, NNMB/BSC-Dust,  
581 DREAM8-NMME and COSMO-MUSCAT models are evaluated against LIRIC results.  
582 The main focus is at Granada station since this site presents a larger number of mineral dust  
583 profiles due to the characteristics of the mineral dust event and allows evaluating the  
584 temporal evolution of the dust microphysical properties.

585 Figure 11 shows the dust mass concentration profiles provided by the four models  
586 and LIRIC every 3 hours from July 9 at 15:00 to July 11 at 18:00. From the profiles  
587 presented in Figure 12,  $C_m$ , the integrated mass concentration for each profile and the  
588 correlation coefficient, R, between LIRIC and the different models are calculated and  
589 presented in Figure 12. Figure 13 shows the profiles of statistical parameters such as R  
590 obtained for LIRIC and the models time series, RMSE, NMB and NMSD, calculated as  
591 described in Section 3 for every altitude level. This three figures needs to be analyzed and  
592 discussed as a whole in order to cover all aspects of the model performance regarding the  
593 temporal and vertical coordinates. An independent interpretation of each of the presented  
594 statistical parameters might be misleading at some points and lead to erroneous  
595 conclusions.

596 According to Figures 11, 12 and 13, BSC-DREAM8b shows a good temporal  
597 correlation with LIRIC, providing larger values on July 9 than on July 10 and 11, as  
598 observed in the experimental data. The correlation coefficient R between BSC-DREAM8b

599 and LIRIC time series is larger than 0.5 for most of the altitudes (Figure 13a). However, the  
600 model strongly underestimates the aerosol load during the three studied days, as indicated  
601 by the NMB in Figure 13c. Positive and larger than 0.5 values of R and the small difference  
602 between LIRIC and BSC-DREAM8b values of  $C_m$  during most of the analyzed period in  
603 Figure 12 indicate that BSC-DREAM8b provides a good estimation of the mineral dust  
604 vertical distribution.

605 A relatively good performance of DREAM8-NMME is observed up to July 10 at  
606 06:00 UTC, when  $\tau_{440nm}$  was larger than 0.2. During this period the model captured quite  
607 well the maximum values and the aerosol load as observed in Figure 11 and indicated by  
608 the integrated mass concentration values in Figure 12, close to those obtained with LIRIC.  
609 Despite this good performance during the first part of the analyzed period, NMB values in  
610 figure 13c suggest an overall underestimation of the aerosol load below 5000 m asl, where  
611 it is higher, and overestimation above 5000 m asl, where concentration values are lower  
612 according to LIRIC. From 3500 m asl, good temporal correlation is observed between  
613 LIRIC and DREAM8-NMME, but R goes close to 0 below this altitude (Figure 13a).  
614 Regarding the vertical distribution of the load,  $C_m$  values in Figure 12 present very small  
615 differences with LIRIC before July 10 at 06:00, but this difference increased afterwards.  
616 Absolute values of R in figure 12 are usually larger than 0.5 and larger than those retrieved  
617 for the other models, indicating good correlation. However, they oscillate from negative to  
618 positive values, indicating a vertical shift in the location of the dust layers during some of  
619 the analyzed periods.

620 NMMB/BSC-Dust shows better performance on July 9, with  $\tau_{440nm}$  values around 0.3,  
621 especially in the layer between 2500-6000 m asl. The difference between LIRIC and the  
622 model integrated mass concentration is also lower during July 9. However, in general the  
623 model tend to underestimate the aerosol load below 4.5 km asl (Figure 13c).  
624 Overestimation of the mass concentration is observed above this altitude though.  
625 NMMB/BSC-Dust correctly follows the aerosol load decrease with time as indicated by  
626 positive correlation values in Figure 13a, but it presents lower temporal correlation  
627 compared to the other models (except for COSMO-MUSCAT). Values of  $C_m$  in Figure 12  
628 are close to those of LIRIC indicating that it correctly forecast the location of the aerosol  
629 load. Nonetheless, low values of R indicate that the vertical distribution of the aerosol

630 layers needs to be improved. For this model it is worthy to point out the un-realistic  
631 increasing maximum at 5000 m asl at 15:00 and 18:00 on July 10 (Figure 11). However,  
632 this maximum is very similar to the one provided by LIRIC between 06:00 and 12:00 UTC.  
633 Therefore, it could be due to a time shift of the model when compared to the LIRIC values.  
634 To check this hypothesis, correlation between LIRIC and the models considering a 3 hours  
635 delay is calculated (Supplementary Figure S5). Correlation between LIRIC and  
636 NMMB/BSC-Dust for simultaneous data is on average below 0.5 (Figure 13a), indicating  
637 that the model does not reproduce very well the temporal evolution of the dust profiles.  
638 This correlation slightly increases between 3500 and 4500 m asl when considering a 3  
639 hours delay between LIRIC and the model, but decreases at the other altitudes. Therefore, it  
640 does not appear to be a systematic delay between the model and LIRIC profiles. However,  
641 in the future it will be beneficial for the modeling community to gather a more extended  
642 database of continuous lidar measurements with similar characteristics to the one presented  
643 here in order to further explore and improve the possible existence of delays between the  
644 models forecast and experimental data.

645 COSMO-MUSCAT shows an increase in the mineral dust load during the analyzed  
646 period with an increasing maximum approximately located between 4 and 5 km. This  
647 behavior is totally opposite to the one observed in LIRIC profiles that show a decrease of  
648 the volume concentration with time, as indicated by the negative values of R in Figure 13a.  
649 According to the integrated mass concentration values in Figure 12, COSMO-MUSCAT  
650 underestimates the dust load during the first half of the analyzed period, whereas an  
651 overestimation of the dust load occurs in the second half. These two opposite behaviors  
652 seem to cancel and, as a result, NMB values in Figure 13c are closer to zero below 4 km  
653 than for the other models, leading to erroneous conclusions. The location of  $C_m$  and R  
654 values in Figure 12 indicate a good performance of the model regarding vertical  
655 distribution on July 9, 11 and the afternoon of July 10. Again, negative R values indicate a  
656 vertical shift in the location of the maximum concentration values during some periods, as  
657 observed also in Figure 11.

658 The four models have shown to have advantages and disadvantages, but a clear  
659 superior performance of any of the four has not been observed. As a general result, the four  
660 models tend to underestimate LIRIC values during the whole period, except for COSMO-

661 MUSCAT that clearly overestimate the dust mass concentration from the afternoon of July  
662 10 onwards. DREAM8-NMME and NMMB/BSC-Dust show a better performance, both  
663 regarding the dust load and the temporal evolution of the event when the aerosol load  
664 observed with the ground-based instrumentation is higher. The temporal evolution of the  
665 event is mostly followed by the BSC models (namely BSC-DREAM8b, DREAM8-NMME  
666 and NMMB/BSC-Dust models) as indicated by the positive correlation with LIRIC time  
667 series, whereas COSMO-MUSCAT shows an opposite behavior (Figure 13a). BSC-  
668 DREAM8b shows the minimum values of the RMSE below 4 km, where most of the  
669 aerosol load is located, and maximum values are obtained for DREAM8-NMME. However,  
670 no statistically significant difference between the models is clearly observed. BSC-  
671 DREAM8b, DREAM8-NMME and COSMO-MUSCAT are not able to capture the high  
672 temporal variability observed with LIRIC, as indicated by the large absolute values of  
673 NMSD in Figure 13d. They range between -0.5 and -1 below 6 km asl for COSMO-  
674 MUSCAT and BSC-DREAM8b and between -1 in the lower altitudes to 2 at the upper  
675 levels for DREAM8-NMME. NMMB/BSC-Dust shows a good performance in this case  
676 with values close to 0 from 3 km upwards.

677 The location of  $C_m$ , which is an indicator of the vertical distribution of the dust mass  
678 concentration, is similar in the case of LIRIC and the models (Figure 12). Despite the  
679 models were capable to reproduce the temporal evolution of  $C_m$ , in general they tended to  
680 locate the dust load at higher altitudes, as indicated by the larger values of  $C_m$  obtained.  
681 Discrepancies are especially relevant in the case of DREAM8-NMME after July 10 in the  
682 afternoon. During this event, BSC-DREAM8b model presented the lowest differences with  
683 LIRIC regarding  $C_m$  height. COSMO-MUSCAT and NMMB/BSC-Dust presented the  
684 lower discrepancies on July 11. These results are comparable to those in the study by  
685 Biniotoglou et al., [2015].

686 Even though they forecast the  $C_m$  fairly well, the analyzed models provided much  
687 smoother profiles than the ones retrieved with LIRIC, with usually a single-broad  
688 maximum located at different altitudes depending on the model. This result is not  
689 surprising due to the coarser vertical resolution of the models compared to lidar profiles,  
690 which can provide more detailed information about the vertical structures of mineral dust.  
691 The vertical correlation between the models, shown in Figure 12b, oscillates between



692 positive and negative values, indicating a shift in the location of the maximum peaks in  
693 those cases when it is negative. R values range between 0.01 and 0.85 in absolute value.  
694 The correlation obtained in the present analysis is lower than the ones presented in  
695 Biniotoglou et al., [2015], where most of the data presented determination coefficient ( $R^2$ )  
696 values above 0.5. This is related to the fact that in the study by Biniotoglou et al., [2015]  
697 selected mineral dust events with higher aerosol load ( $\tau_{440}>0.15$ ) were presented whereas in  
698 this study the continuous evolution of the dust event was analyzed with  $\tau_{440}$  ranging  
699 between 0.07 and 0.40. Therefore, according to the present study models seem to show a  
700 better performance in cases of higher aerosol load.

701 [Figure 11]

702 [Figure 12]

703 [Figure 13]

704

705 Model profiles were also obtained at the stations of Athens, Barcelona, Bucharest and  
706 Évora in order to evaluate their performance at stations where there is a slight or no  
707 presence of mineral dust. At Athens (Figure S1 from Supplementary material) almost  
708 negligible mass concentration values were forecast by the different models, with the  
709 exception of DREAM8-NMME. This model indicated the presence of mineral dust in mass  
710 concentrations up to  $100 \mu\text{g}\cdot\text{m}^{-3}$  reaching 4000 m asl on July,10 and up to  $65 \mu\text{g}\cdot\text{m}^{-3}$  on the  
711 July 11 which is not in agreement with LIRIC results. In spite of the disagreement, it is  
712 worthy to point out that the dust layer observed at Athens between 3000 and 5000 m asl on  
713 July 11 according to LIRIC data was correctly forecast by the different models. At  
714 Barcelona station (Figure S2), DREAM8-NMME were not in agreement with the  
715 experimental results since it forecasted dust mass concentrations of up to  $100 \mu\text{g}\cdot\text{m}^{-3}$  and  
716 located below 2000 m asl. At Bucharest (Figure S3), large dust concentrations were  
717 forecasted between 3000 and 7000 m asl by BSC-DREAM8b, DREAM8-NMME and  
718 NMMB/BSC-Dust on July 9. On July 10 and 11 the dust load forecasted by the models  
719 was much lower, even though it reached up to  $50 \mu\text{g}\cdot\text{m}^{-3}$ . This is not in agreement with our  
720 experimental results since only coarse spherical and fine particles and no mineral dust  
721 should be forecasted here. Finally, at Évora station (Figures S4), DREAM8-NMME

722 forecasted dust mass concentration lower than  $10 \mu\text{g}\cdot\text{m}^{-3}$  below 2000 m asl COSMO-  
723 MUSCAT forecasted similar concentrations above 2000 m asl These mass concentration  
724 values are almost negligible and therefore good agreement can be considered. In general,  
725 good results were provided by the different models at the five stations. However,  
726 DREAM8-NMME seems to be overestimating the dust mass concentrations at those  
727 stations affected by aerosol types different to mineral dust.

728 An in-depth analysis of the causes for the discrepancies between the models and  
729 LIRIC is out of the scope of this study, especially taking into account that they showed a  
730 similar performance here, with none of them proving to be more accurate than the others. In  
731 general we observed that the BSC models showed a similar behavior when compared with  
732 COSMO-MUSCAT, based on a different philosophy. However, none of them showed a  
733 statistically significant better performance. Differences between the obtained results lie on  
734 the different approaches used in the different models, the different meteorological fields  
735 used, dust sources, horizontal and vertical transport schemes, different resolutions, etc., as  
736 already pointed out in Binietoglou et al., [2015]. Robust conclusions at this respect cannot  
737 be withdrawn from this study and would require wider databases with higher temporal and  
738 spatial coverage in order to cover the different aspects of the model calculations and more  
739 dedicated studies. Nonetheless, the comparison presented here provided valuable results  
740 since it addresses the points of discrepancy and proves LIRIC potential as a tool for future  
741 model evaluations. Information inferred from the results obtained here could be used for the  
742 planning of future validation strategies and campaigns management.

743

## 744 5. SUMMARY AND CONCLUSIONS

745

746 In this study, the characterization of aerosol microphysical properties at different stations  
747 throughout Europe was performed in the framework of the ChArMEx/EMEP 2012 field  
748 campaign, in support to which EARLINET lidar stations performed continuous  
749 measurements during the 72 hours. LIRIC profiles were obtained at five different stations  
750 in Europe (i.e. Athens, Barcelona, Bucharest, Évora and Granada) in order to characterize  
751 atmospheric aerosol particles both in the vertical and horizontal coordinates and also their

752 temporal evolution during this period. From the analysis of the aerosol microphysical  
753 properties at the different stations, two different aerosol plumes were clearly observed: one  
754 affecting the Western Mediterranean region, loaded with mineral dust, and another one over  
755 the Balkans area, mainly composed of fine particles and coarse spherical particles. Granada  
756 station was clearly affected by the mineral dust outbreak during these 72 hours, whereas  
757 mainly aerosol from local origin was affecting Évora and Barcelona. The dust plume was  
758 also observed above Barcelona on July 11. A mixture of fine and coarse spherical particles  
759 was observed over Bucharest, likely related to the presence of smoke from European fires,  
760 whereas at Athens mainly fine particles were observed, except on July 11, when mineral  
761 dust of different origin from the one in Granada and Barcelona was observed at 3.5 km asl  
762 as indicated by the backward trajectories analysis.

763 A thorough evaluation of the temporal evolution and the aerosol layers dynamics was  
764 possible at Granada station, where a total of 60 lidar profiles every 30-min and 21  
765 AERONET inversion retrievals were available. The analysis of the microphysical  
766 properties profiles retrieved with LIRIC indicated that the dust event was decreasing in  
767 intensity, with larger concentrations on July 9 ( $\sim 35 \mu\text{m}^3 \cdot \text{cm}^{-3}$ ) decreasing towards July 11  
768 ( $\sim 15 \mu\text{m}^3 \cdot \text{cm}^{-3}$ ), in agreement with AERONET and satellite data. On July 9 there was a  
769 strong predominance of the coarse spheroid mode with maximum values in the afternoon  
770 while an increase in the concentration of the coarse spheroid mode up to  $15 \mu\text{m}^3 \cdot \text{cm}^{-3}$  was  
771 observed during the afternoon of July 11. This temporal evolution of the microphysical  
772 properties reveals possible aging processes of the mineral dust above the station or even  
773 mixing processes with different aerosol types.

774 These results provide a good overview of the aerosol microphysical properties in the  
775 Mediterranean region during ChArMEx campaign. They also highlight the importance of  
776 having combined regular AERONET/EARLINET measurements for the characterization of  
777 aerosol microphysical properties in the vertical, horizontal and spatial coordinates with high  
778 resolution by means of algorithms such as LIRIC and suggest the importance of extending  
779 this kind of measurements. Our study remarks the capability of LIRIC to be implemented in  
780 a simple, automated and robust way within a network such as EARLINET and during  
781 special measurement campaigns obtaining reliable results. In addition, the advantages on  
782 the use of depolarization measurements with lidar systems are also emphasized here, since

783 the stations with depolarization capabilities (namely Bucharest, Évora and Granada)  
784 provided much more complete information about the microphysical properties profiles.

785 The availability of LIRIC output profiles at the five different stations provided  
786 regional coverage and made possible a comparison with the modelled dust fields provided  
787 by BSC-DREAM8b, NMMB/BSC-Dust, DREAM8-NMME and COSMO-MUSCAT. The  
788 regional comparison revealed quite good agreement with the horizontal distribution of the  
789 dust plume forecast by models (based on a similar philosophy), but lower agreement for  
790 COSMO-MUSCAT over the Balkans region.

791 A more detailed comparison using dust mass concentration profiles derived every 3  
792 hours from 06:00 to 18:00 UTC over the 3 days of interest was also performed. The four  
793 models tended to underestimate the dust mass concentration when compared to LIRIC  
794 results, except for COSMO-MUSCAT on the afternoon of July 10 and on July 11 that  
795 overestimated it. The overall underestimation of the dust mass concentration was between  
796 80 and 100% for altitudes below 4 km depending on the model. Above this altitude,  
797 DREAM8-NMME and NMMB/BSC-Dust tended to overestimate the dust mass  
798 concentration values reaching up to 150% overestimation. The agreement between LIRIC  
799 and the models was better when determining the vertical location of the mineral dust load,  
800 even though the models tended to locate the mineral dust at higher altitudes than seen by  
801 lidar, as indicated by the determination coefficient values and the center of mass location.  
802 The correlation coefficient between LIRIC and the models reached absolute values of up to  
803 0.85, even though in most of the cases the maximum peaks were shifted when compared  
804 to LIRIC showing anticorrelation. The difference in the center of mass location was below  
805 1 km in 65% of the cases.

806 A comparison between LIRIC and the models was also performed at the stations of  
807 Évora, Barcelona, Athens and Bucharest. In general, good agreement was obtained for  
808 BSC-DREAM8b, NMMB/BSC-Dust and COSMO-MUSCAT when no dust is observed.  
809 DREAM8-NMME indicated the presence of mineral dust in large concentrations in Athens,  
810 Barcelona and Évora, opposite to LIRIC results, which indicated and almost negligible or  
811 no presence of mineral dust. BSC-DREAM8b, NMMB/BSC-Dust and DREAM8-NMME  
812 forecast the presence of mineral dust in the vertical coordinate in Bucharest station, where  
813 LIRIC indicated the presence of a different aerosol type (mostly fine and spherical

814 particles), suggesting that COSMO-MUSCAT philosophy is more adequate for this specific  
815 case and location.

816 The four analyzed models present advantages and disadvantages but none of them  
817 showed a statistically significant better performance when evaluated against LIRIC results.  
818 In general, the three BSC models showed more similar results compared against COSMO-  
819 MUSCAT, based on a different philosophy. But further conclusions regarding the  
820 differences between the models cannot be withdrawn from our study. A more detailed  
821 analysis based on a wider and more specific database designed to cover the different  
822 aspects of the model calculations would be required. Results presented here are valuable  
823 since they prove LIRIC potential as a tool for model evaluation and provide valuable  
824 information for the planning of future validation strategies and campaign management.

825

## 826 Acknowledgements

827 This work was supported by the Andalusia Regional Government through projects P12-  
828 RNM-2409 and P10-RNM-6299, by the Spanish Ministry of Economy and  
829 Competitiveness through projects TEC2012-34575, TEC2015-63832-P, CGL2013-45410-  
830 R, CGL2011-13580-E/CLI, CGL2011-16124-E, and CGL2013-46736-R; by the Spanish  
831 Ministry of Science and Innovation (project UNPC10-4E-442); the EU through the H2020  
832 project ACTRIS2 (contract number 654109); by the University of Granada through the  
833 contract “Plan Propio. Programa 9. Convocatoria 2013”; and by the Department of  
834 Economy and Knowledge of the Catalan autonomous government (grant 2014 SGR 583).  
835 M. J. Granados-Muñoz was funded under grant AP2009-0552 from the Spanish Ministry of  
836 Education and Science. S. N. Pereira was funded under fellowship SFRH/BPD/81132/2011  
837 and projects FCOMP-01-0124-FEDER-029212 (PTDC/GEO-MET/4222/2012 from the  
838 Portuguese Government). S. Basart and J.M. Baldasano acknowledge the CICYT project  
839 (CGL2010-19652 and CGL2013-46736) and Severo Ochoa Programme (SEV-2011-00067)  
840 of the Spanish Government. BSC-DREAM8b and NMMB/BSC-Dust simulations were  
841 performed on the Mare Nostrum supercomputer hosted by Barcelona Supercomputing  
842 Center-Centro Nacional de Supercomputación (BSC-CNS). This paper was realized also as  
843 a part of the project III43007 financed by the Ministry of Education and Science of the

844 Republic of Serbia within the framework of integrated and interdisciplinary research for the  
845 period 2011-2015. It has also received funding from the European Union's Seventh  
846 Framework Programme for research, technological development and demonstration under  
847 grant agreement no 289923 - ITaRS. The CIMEL Calibration was performed at the  
848 AERONET-EUROPE calibration center, supported by ACTRIS-2 (EUH2020 grant  
849 agreement No 654109. The authors express gratitude to the NOAA Air Resources  
850 Laboratory for the HYSPLIT transport and dispersion model; the ICARE Data and Services  
851 Center the MODIS team; and the ChArMEx project of the multidisciplinary research  
852 programme MISTRALS (Mediterranean Integrated Studies at Regional And Local Scales;  
853 <http://www.mistrals-home.org>).

#### 854 References

- 855 Alfaro, S., and Gomes, L.: Modeling mineral aerosol production by wind erosion:  
856 intensities and aerosol size distribution in source areas, *J. Geophys. Res.*, 106, 18075-  
857 18084, doi:10.1029/2000JD900339, 2001.
- 858 Andreae, M.: Biomass burning: Its history, use, and distribution and its impact on  
859 environmental quality and global climate, in *Global Biomass Burning- Atmospheric,*  
860 *Climatic, and Biospheric Implications*, Levine, J.S., editor, MIT Press, Cambridge, MA, 3-  
861 21, 1991.
- 862 Basart, S., Pérez, C., Cuevas, E., Baldasano, J. M., and Gobbi, G. P.: Aerosol  
863 characterization in Northern Africa, Northeastern Atlantic, Mediterranean Basin and  
864 Middle East from direct-sun AERONET observations, *Atmos. Chem. Phys.*, 9, 8265–8282,  
865 doi:10.5194/acp-9-8265-2009, 2009.
- 866 Basart, S., Pérez, C., Nickovic, S., Cuevas, E., and Baldasano, J. M.: Development and  
867 evaluation of the BSC-DREAM8B dust regional model over Northern Africa, the  
868 Mediterranean and the Middle East, *Tellus B*, 64, 18539,  
869 <http://dx.doi.org/10.3402/tellusb.v64i0.18539>, 2012.
- 870 Binietoglou, I., Basart S., Alados-Arboledas, L., Amiridis, V., Argyrouli, A., Baars, H.,  
871 Baldasano, J. M., Balis, D., Belegante, L., Bravo-Aranda, J. A., Burlizzi, P., Carrasco, V.,  
872 Chaikovsky, A., Comerón, A., D'Amico, G., Filioglou, M., Granados-Muñoz, M. J.,  
873 Guerrero-Rascado, J. L., Ilic, L., Kokkalis, P., Maurizi, A., Mona, L., Monti, F., Muñoz-  
874 Porcar C., Nicolae, D., Papayannis, A., Pappalardo, G., Pejanovic, G., Pereira, S. N.,  
875 Perrone, M. R., Pietruczuk, A., Posyniak, M., Rocadenbosch, F., Rodríguez-Gómez, A.,  
876 Sicard, M., Siomos, N., Szkop, A., Terradellas, E., Tsekeri, A., Vukovic, A., Wandinger,  
877 U., and Wagner, J.: A methodology for investigating dust model performance using  
878 synergistic EARLINET/AERONET dust concentration retrievals, *Atmos. Meas. Tech.*  
879 *Disc.*, 8, 3605-3666, doi:10.5194/amtd-8-3605-2015, 2015.
- 880 Bravo-Aranda, J. A., Navas-Guzmán, F., Guerrero-Rascado, J. L., Pérez-Ramírez, D.,  
881 Granados-Muñoz, M. J., and Alados-Arboledas, L.: Analysis of lidar depolarization

882 calibration procedure and application to the atmospheric aerosol characterization, *Int. J.*  
883 *Remote Sens.*, 34, 3543-3560, doi: 10.1080/01431161.2012.716546, 2013.

884 Bosenberg, J., Matthias ,V., Amodeo ,A., Amiridis ,V., Ansmann ,A., Baldasano, J. M.,  
885 Balin, I., Balis, D., Bockmann, C., Boselli, A., Carlsson, G., Chaikovsky, A., Chourdakis,  
886 G., Comeron, A., De Tomasi, F., Eixmann, R., Freudenthaler, V., Giehl, H., Grigorov, I.,  
887 Hagard, A., Iarlori, M., Kirsche, A., Kolarov, G., Komguem, L., Kreipl, S., Kumpf, W.,  
888 Larcheveque, G., Linne, H., Matthey, R., Mattis, I., Mekler, A., Mironova, I., Mitev, V.,  
889 Mona, L., Muller, D., Music, S., Nickovic, S., Pandolfi, M., Papayannis, A., Pappalardo,  
890 G., Pelon, J., Pérez, C., Perrone, M. R., Persson, R., Resendes, D. P., Rizi, V.,  
891 Rocadenbosch, F., Rodrigues, J. A., Sauvage, L., Schneidenbach, L., Schumacher, R.,  
892 Shcherbakov, V., Simeonov, V., Sobolewski, P., Spinelli, N., Stachlewska, I., Stoyanov,  
893 D., Trickl, T., Tsaknakis, G., Vaughan, G., Wandinger, U., Wang, X., Wiegner, M.,  
894 Zavrtnik, M., and Zerefos, C.: EARLINET: A European Aerosol Research Lidar Network  
895 to Establish an Aerosol Climatology, Max-Planck Institute für Meteorologie, Report No.  
896 348, ISSN 0937 1060, 2003.

897

898 Bréon, F.-M.: How do aerosols affect cloudiness and climate?, *Science*, 313, 623-624,  
899 doi:10.1126/science.1131668, 2006.

900

901 Buzzi, A., D'Isidoro, M., and Davolio, S.: A case-study of an orographic cyclone south of  
902 the Alps during the MAP SOP, *Quarterly J. Royal Meteor. Soc.*, 129, 1795-1818, 2003.

903

904 Carrer, D., Ceamanos, X., Six, B., and Roujean J.-L. (2014) AERUS-GEO: A newly  
905 available satellite-derived aerosol optical depth product over Europe and Africa, *Geophys.*  
906 *Res. Lett.*, 41, 7731–7738, doi:[10.1002/2014GL061707](https://doi.org/10.1002/2014GL061707).

907

908 Claquin, T., Schulz, M., Balkanski, Y., and Boucher, O.: Uncertainties in assessing  
909 radiative forcing by mineral dust, *Tellus B*, 50, 491-505, doi:10.1034/j.1600-  
910 0889.1998.t01-2-0000, 1998.

911 Chaikovsky, A., O. Dubovik, P. Goloub, N. Balashevich, A. Lopatsin, Y. Karol, S. Denisov  
912 and T. Lapyonok (2008). Software package for the retrieval of aerosol microphysical  
913 properties in the vertical column using combined lidar/photometer data (test version).  
914 Technical Report. Minsk, Belarus, Institute of Physics, National Academy of Sciences of  
915 Belarus

916 Chaikovsky, A., O. Dubovik, P. Goloub, D. Tanré and G. Pappalardo, Wandinger, U.,  
917 Chaikovskaya, L., Denisov, S., Grudo, Y., Lopatsin, A., Karol, Y., Lapyonok, T., Korol,  
918 M., Osipenko, F., Savitski, D., Slesar, A., Apituley, A., Arboledas, L. A., Biniotoglou, I.,  
919 Kokkalis, P., Granados Muñoz, M. J., Papayannis, A., Perrone, M. R., Pietruczuk, A.,  
920 Pisani, G., Rocadenbosch, F., Sicard, M., De Tomasi, F., Wagner, J., and Wang, X. (2012).  
921 Algorithm and software for the retrieval of vertical aerosol properties using combined  
922 lidar/radiometerdata: Dissemination in EARLINET,. 26th International Laser and Radar  
923 Conference, Porto Heli, Greece.

924 Chaikovsky, A., Dubovik, O., Holben, B., Bril, A., Goloub, P., Tanré, D., Pappalardo, G.,  
925 Wandinger, U., Chaikovskaya, L., Denisov, S., Grudo, J., Lopatin, A., Karol, Y.,  
926 Lapyonok, T., Amiridis, V., Ansmann, A., Apituley, A., Allados-Arboledas, L.,

927 Binietoglou, I., Boselli, A., D'Amico, G., Freudenthaler, V., Giles, D., Granados-Muñoz,  
928 M. J., Kokkalis, P., Nicolae, D., Oshchepkov, S., Papayannis, A., Perrone, M. R.,  
929 Pietruczuk, A., Rocadenbosch, F., Sicard, M., Slutsker, I., Talianu, C., De Tomasi, F.,  
930 Tsekeri, A., Wagner, J., and Wang, X.: Lidar-Radiometer Inversion Code (LIRIC) for the  
931 retrieval of vertical aerosol properties from combined lidar/radiometer data: development  
932 and distribution in EARLINET, *Atmos. Meas. Tech.*, 9, 1181-1205, doi:10.5194/amt-9-  
933 1181-2016, 2016.

934 Chen, Y., and Penner, J. E.: Uncertainty analysis for estimates of the first indirect aerosol  
935 effect. *Atmos. Chem. Phys.*, 5, 2935-2948, doi:10.5194/acp-5-2935-2005, 2005.

936 D'Amico, G., et al., (), EARLINET Single Calculus Chain – general presentation,  
937 methodology and strategy, in prep. for *Atmos. Meas. Tech. Discuss.*, 2015.

938 Draxler, R. R., and Rolph, G. D.: HYSPLIT (HYbrid Single-Particle Lagrangian Integrated  
939 Trajectory) model access via NOAA ARL READY website (<http://www.arl.noaa.gov/ready/hysplit4.html>). NOAA Air Resources Laboratory, Silver Spring, Md, 2003.

940  
941 Dubovik, O., and King, M. D.: A flexible inversion algorithm for retrieval of aerosol  
942 optical properties from Sun and sky radiance measurements, *J. Geophys. Res.*, 105, 20673-  
943 20696, doi: 10.1029/2000JD900282, 2000.

944 Dubovik, O., Sinyuk, A., Lapyonok, T., Holben, B. N., Mishchenko, M., Yang, P., Eck, T.  
945 F., Volten, H., Muñoz, O., and Veihelmann, B.: Application of spheroid models to account  
946 for aerosol particle nonsphericity in remote sensing of desert dust, *J. Geophys. Res.*, 111,  
947 D11208, doi:10.1029/2005JD006619, 2006.

948 Dulac, F.: An overview of the Chemistry-Aerosol Mediterranean Experiment (ChArMEx),  
949 *Proc. EGU Gen. Assem. 2014*, *Geophys. Res. Abst.*, 16, EGU2014-11441, 2014.

950 Eck, T. F., Holben, B. N., Reid, J. S., Dubovik, O., Smirnov, A., O'Neill, N. T., Slutsker, I.,  
951 and Kinne, S.: Wavelength dependence of the optical depth of biomass burning, urban, and  
952 desert dust aerosols, *J. Geophys. Res.*, 104(D24), 31333-31349, doi  
953 doi:10.1029/1999JD900923, 1999.

954 Espen Yttri, K., Aas, W., Tørseth, K., Kristiansen, N. I., Lund Myhre, C., Tsyro, S.,  
955 Simpson, D., Bergström, R., Marečková, K., Wankmüller, R., Klimont, Z., Amman, M.,  
956 Kouvarakis, G. N., Laj, P., Pappalardo, G., and Prévôt, A.: EMEP Co-operative Programme  
957 for Monitoring and Evaluation of the Long-Range Transmission of Air Pollutants in  
958 Europe; Transboundary particulate matter in Europe Status report 2012, available at  
959 <http://www.actris.net/Portals/97/documentation/dissemination/other/emep4-2012.pdf> (last  
960 15 access: 9 December 2014), 2012.

961 Estellés, V., Utrillas, M. P., Martínez-Lozano, J. A., Alcántara, A., Alados-Arboledas, L.,  
962 Olmo, F. J., Lorente, J., de Cabo, X., Cachorro, V., Horvath, H., Labajo, A., Sorribas, M.,  
963 Díaz, J. P., Díaz, A. M., Silva, A. M., Elías, T., Pujadas, M., Rodrigues, J.A., Cañada, J.,  
964 and García Y.: Intercomparison of spectroradiometers and Sun photometers for the  
965 determination of the aerosol optical depth during the VELETA-2002 field campaign, *J.*  
966 *Geophys. Res.*, 111, D17207, doi:10.1029/2005JD006047, 2006.

967 Formenti, P., Schütz, L., Balkanski, Y., Desboeufs, K., Ebert, M., Kandler, K., Petzold, A.,  
968 Scheuven, D., Weinbruch, S., and Zhang, D.: Recent progress in understanding physical



969 and chemical properties of African and Asian mineral dust, *Atmos. Chem. Phys.*, 11, 8231-  
970 8256, doi:10.5194/acp-11-8231-2011, 2011.

971 Freudenthaler, V., Esselborn, M., Wiegner, M., Heese, B., Tesche, M., Ansmann, A.,  
972 Müller, D., Althausen, A., Wirth, M., and Fix, A.: Depolarization ratio profiling at several  
973 wavelengths in pure Saharan dust during SAMUM 2006, *Tellus B*, 61, 165-179, doi:  
974 10.1111/j.1600-0889.2008.00396.x, 2009.

975 Gama, C., Tchepel, O., Baldasano, J. M., Basart, S., Ferreira, J., Pio, Cardoso, J., and  
976 Borrego, C.: Seasonal patterns of Saharan dust over Cape Verde-a combined approach  
977 using observations and modelling. *Tellus B* 2015, 67, 24410,  
978 <http://dx.doi.org/10.3402/tellusb.v67.24410>, 2015.

979 Ginoux, P., Chin, M., Tegen, I., Prospero, J. M., Holben, B., Dubovik, O., and Lin, S. J. :  
980 Sources and distributions of dust aerosols simulated with the GOCART model, *J.*  
981 *Geophys. Res.*, 106, 20255-20273, doi: 0148-0227 / 01 / 2000JD 000053509.00, 2011.

982 Gomes, L., Bergametti, G., Coudé-Gaussen, G., and Rognon, P.: Submicron desert dusts: a  
983 sandblasting process, *J. Geophys. Res.*, 95, 13927-13935, doi:10.1029/JD095iD09p13927,  
984 1990.

985 Granados-Muñoz, M. J., Bravo-Aranda, J. A., Baumgardner, D., Guerrero-Rascado, J. L.,  
986 Pérez-Ramírez, D., Navas-Guzmán, F., Veselovskii, I., Lyamani, H., Valenzuela, A., Olmo,  
987 F.J., Titos, G., Andrey, J., Chaikovsky, A., Dubovik, O., Gil-Ojeda, M., and Alados-  
988 Arboledas, L. (2015). Study of aerosol microphysical properties profiles retrieved from  
989 ground-based remote sensing and aircraft in-situ measurements during a Saharan dust  
990 event. *Atmos. Meas. Tech. Discuss.*, 8(9), 2015.

991 Granados-Muñoz, M. J., Guerrero-Rascado, J. L., Bravo-Aranda, J. A., Navas-Guzmán, F.,  
992 Valenzuela, A., Lyamani, H., Chaikovsky, A., Wandinger, U., Ansmann, A., Dubovik, O.,  
993 Grudo, J. O., and Alados-Arboledas, L.: Retrieving aerosol microphysical properties by  
994 Lidar-Radiometer Inversion Code (LIRIC) for different aerosol types, *J. Geophys. Res.*  
995 *Atmos.*, 119, 4836-4858 doi:10.1002/2013JD021116, 2014.

996 Granados-Muñoz, M. J., Navas-Guzmán, F., Bravo-Aranda, J. A., Guerrero-Rascado, J. L.,  
997 Lyamani, H., Fernández-Gálvez, J., and Alados-Arboledas, L.: Automatic determination of  
998 the planetary boundary layer height using lidar: One-year analysis over southeastern Spain,  
999 *J. Geophys. Res.*, 117, D18208, doi:10.1029/2012JD017524, 2012.

1000 Guerrero-Rascado, J. L., F. J. Olmo, I. Avilés-Rodríguez, F. Navas-Guzmán, D. Pérez-  
1001 Ramírez, H. Lyamani and L. Alados-Arboledas (2009). Extreme Saharan dust event over  
1002 the southern Iberian Peninsula in September 2007: Active and passive remote sensing from  
1003 surface and satellite, *Atmos. Chem. Phys.*, 9, 8453-8469.

1004 Guerrero-Rascado, J. L., Landulfo, E., Antuña, J. C., Barbosa, H. M. J., Barja, B., Bastidas,  
1005 A. E., Bedoya, A. E., da Costa, R., Estevan, R., Forno, R. N., Gouveia, D. A., Jiménez, C.,  
1006 Larroza, E. G., Lopes, F. J. S., Montilla-Rosero, E., Moreira, G. A., Nakaema, W. M.,  
1007 Nisperuza, D., Otero, L., Pallotta, J. V., Papandrea, S., Pawelko, E., Quel, E. J., Ristori, P. ,  
1008 Rodrigues, P. F., Salvador, J., Sánchez, M. F., and Silva, A.: Towards an instrumental  
1009 harmonization in the framework of LALINET: dataset of technical specifications, *Proc.*  
1010 *SPIE* 2014, vol. 9246, 924600-1—924600-14, doi: 10.1117/12.2066873 , 2014.

1011 Haustein K., Pérez, C., Baldasano, J. M., Jorba, O., Basart, S., Miller, R. L., Janjic, Z.,  
1012 Black, T., Nickovic, S., Todd, M. C. and Washington, R.: Atmospheric dust modeling from  
1013 meso to global scales with the online NMMB/BSC-Dust model—Part 2: Experimental  
1014 campaigns in Northern Africa, *Atmos. Chem. Phys.* 12, 2933–2958, doi:10.5194/acp-12-  
1015 2933-2012, 2012.

1016 Heinold, B., Tegen, I., Schepanski, K., Tesche, M., Esselborn, M., Freudenthaler, V.,  
1017 Gross, S., Kandler, K., Knippertz, P., and Müller, D.: Regional modelling of Saharan dust  
1018 and biomass-burning smoke, *Tellus B*, 63, 781-799, doi:10.1111/j.1600-  
1019 0889.2011.00570.x, 2011a.

1020 Heinold, B., Tegen, I., Esselborn, M., Kandler, K., Knippertz, P., Müller, D., Schladitz, A.,  
1021 Tesche, M., Weinzierl, B., Ansmann, A., Althausen, D., Laurent, B., Petzold, A., and  
1022 Schepanski, K.: Regional Saharan dust modelling during the SAMUM 2006 campaign,  
1023 *Tellus B*, 61, 307-324, doi: 10.1111/j.1600-0889.2008.00387.x, 2009.

1024 Holben, B. N., Eck, T. F., Slutsker, I., Tanré, D., Buis, J. P., Setzer, A., Vermote, E.,  
1025 Reagan, J.A., Kaufman, Y. J., Nakajima, T., Lavenus, F., Jankowiak I., and Smirnov, A.:  
1026 AERONET – A federated instrument network and data archive for aerosol characterization,  
1027 *Remote Sens. Environ.*, 66, 1–16, 1998.

1028 Huang, J., Q. Fu, J. Su, Q. Tang, P. Minnis, Y. Hu, Y. Yi, and Zhao, Q.: Taklimakan dust  
1029 aerosol radiative heating derived from CALIPSO observations using the Fu-Liou radiation  
1030 model with CERES constraints, *Atmos. Chem. Phys.*, 9, 4011-4021, doi:10.5194/acp-9-  
1031 4011-2009, 2009.

1032 IPCC: Contribution of Working Group I to the Fifth Assessment Report of the  
1033 Intergovernmental Panel on Climate Change. Summary for Policymakers in Climate  
1034 Change, Stocker, Cambridge University Press, 2013.

1035 Janjic, Z. I., Gerrity Jr, J. P., and Nickovic, S.: An alternative approach to nonhydrostatic  
1036 modeling, *Mon. Weather Rev.*, 129, 1164-1178, 2001.

1037 Knoth, O., and Wolke, R.: An explicit-implicit numerical approach for atmospheric  
1038 chemistry-transport modelling, *Atmos. Environ.*, 32, 1785-1797, 1998.

1039 Kokkalis, P., A. Papayannis, V. Amiridis, R. E. Mamouri, I. Veselovskii, A. Kolgotin, G.  
1040 Tsaknakis, N. I. Kristiansen, A. Stohl and L. Mona (2013). Optical, microphysical, mass  
1041 and geometrical properties of aged volcanic particles observed over Athens, Greece, during  
1042 the Eyjafjallajökull eruption in April 2010 through synergy of Raman lidar and  
1043 sunphotometer measurements, *Atmosp. Chem. Phys.*, 13, 9303-9320, doi:10.5194/acp-13-  
1044 9303-2013, 2013.

1045 Kokkalis, P., A. Papayannis, R. E. Mamouri, G. Tsaknakis, V. Amiridis (2012). The EOLE  
1046 lidar system of the National Technical University of Athens, 629-632, 26<sup>th</sup> International  
1047 Laser Radar Conference, 25-29 June 2012, Porto Heli, Greece.

1048 Kumar, D., F. Rocadenbosch, M. Sicard, A. Comeron, C. Muñoz, D. Lange, S. Tomás and  
1049 E. Gregorio (2011). Six-channel polychromator design and implementation for the UPC  
1050 elastic/Raman LIDAR, *Proc. SPIE*, 8182, pp. 81820W-1-10.

1051 Laurent, B., Tegen, I., Heinold, B., Schepanski, K., Weinzierl, B., and Esselborn, M.: A  
1052 model study of Saharan dust emissions and distributions during the SAMUM-1 campaign.  
1053 *J. Geophys. Res.*, 115, D21210, doi:10.1029/2009JD012995, 2010.

- 1054 Lopatin, A., Dubovik, O., Chaikovsky, A., Goloub, P., Lapyonok, T., Tanré, D., and  
1055 Litvinov, P.: Enhancement of aerosol characterization using synergy of lidar and sun-  
1056 photometer coincident observations: the GARRLiC algorithm, *Atmos.Meas. Tech.*, 6,  
1057 2065-2088, doi:10.5194/amt-6-2065-2013, 2013.
- 1058 Lyamani, H., A. Valenzuela, D. Perez-Ramirez, C. Toledano, M. J. Granados-Muñoz, F. J.  
1059 Olmo and L. Alados-Arboledas: Aerosol properties over the western Mediterranean Basin:  
1060 temporal and spatial variability. *Atmos. Chem. Phys.*, 15, 2473-2486, doi:10.5194/acp-15-  
1061 2473-2015, 2015.
- 1062 Mamouri, R. E. and Ansmann, A.: Fine and coarse dust separation with polarization lidar,  
1063 *Atmos. Meas. Tech.*, 7, 3717-3735, doi:10.5194/amt-7-3717-2014, 2014.
- 1064 Mattis, I., Ansmann, A., Müller, D., Wandinger, U., and Althausen, D. (2004), Multiyear  
1065 aerosol observations with dual-wavelength Raman lidar in the framework of EARLINET,  
1066 *J. Geophys. Res.*, 109, D13203, doi:10.1029/2004JD004600, 2004.
- 1067 Maurizi, A., D'Isidoro, M., and Mircea, M.: BOLCHEM: An Integrated System for  
1068 Atmospheric Dynamics and Composition, in *Integrated Systems of Meso-Meteorological  
1069 and Chemical Transport Models*, Baklanov, A., Mahura, A., and Sokhi, R. J., Eds.,  
1070 Springer, 89-94, 2011.
- 1071 McCormick, M. P., Wang, P. H., and Poole, L. R.: Stratospheric aerosols and clouds, in  
1072 *Aerosol-Cloud-Climate Interactions*, Hobbs, P. V. Ed., Academic Press, 205-222, 1993.
- 1073 Mircea, M., D'Isidoro, M., Maurizi, A., Vitali, L., Monforti, F., Zanini, G., and Tampieri,  
1074 F.: A comprehensive performance evaluation of the air quality model BOLCHEM to  
1075 reproduce the ozone concentrations over Italy, *Atmos. Environ.*, 42, 1169-1185,  
1076 doi:10.1016/j.atmosenv.2007.10.043, 2008.
- 1077 Nabat, P., Somot, S., Mallet, M., Sanchez-Lorenzo, A., and Wild, M.: Contribution of  
1078 anthropogenic sulfate aerosols to the changing Euro-Mediterranean climate since 1980,  
1079 *Geophys. Res. Lett.*, 41, 5605-5611, doi:10.1002/2014GL060798, 2014.
- 1080 Nabat, P., Somot, S., Mallet, M., Sevault, F., Chiacchio, M., and Wild, M.: Direct and  
1081 semi-direct aerosol radiative effect on the Mediterranean climate variability using a coupled  
1082 regional climate system model, *Clim. Dyn.*, 44, 1127-1155, doi:10.1007/s00382-014-2205-  
1083 6, 2015.
- 1084 Nakajima, T., Tonna, G., Rao, R., Boi, P., Kaufman, Y., and Holben, B.: Use of sky  
1085 brightness measurements from ground for remote sensing of particulate polydispersions,  
1086 *Appl. Opt.*, 35, 2672-2686, doi:10.1364/AO.35.002672, 1996.
- 1087 Nemuc, A., Vasilescu, J., Talianu, C., Belegante, L., and Nicolae, D.: Assessment of  
1088 aerosol's mass concentrations from measured linear particle depolarization ratio (vertically  
1089 resolved) and simulations, *Atmos. Meas. Tech.*, 6, 3243-3255, doi:10.5194/amt-6-3243-  
1090 2013, 2013.
- 1091 Nickovic, S., Kallos, K., Papadopoulos, A., and Kakaliagou, O.: A model for prediction of  
1092 desert dust cycle in the atmosphere. *J. Geophys. Res.*, 106, 18113-18118, doi:10.1029/  
1093 0227/01/2000JD900794\$09.00, 2001.

1094 Noh, Y. M.: Single-scattering albedo profiling of mixed Asian dust plumes with  
1095 multiwavelength Raman lidar, *Atmos. Environ.*, 95, 305-317,  
1096 doi:10.1016/j.atmosenv.2014.06.028, 2014.

1097 Olmo, F. J., Quirantes, A., Alcántara, A., Lyamani, H., and Alados-Arboledas, L.:  
1098 Preliminary results of a non-spherical aerosol method for the retrieval of the atmospheric  
1099 aerosol optical properties, *J. Quant. Spectrosc. Radiat. Transf.*, 100, 305-314, doi:  
1100 [10.1016/j.jqsrt.2005.11.047](https://doi.org/10.1016/j.jqsrt.2005.11.047), 2006.

1101 Papayannis, A., Amiridis, V., Mona, L., Tsaknakis, G., Balis, D., Bösenberg, J.,  
1102 Chaikovski, A., De Tomasi, F., Grigorov, I., Mattis, I., Mitev, V., Müller, D., Nickovic, S.,  
1103 Pérez, C., Pietruczuk, A., Pisani, G., Ravetta, F., Rizi, V., Sicard, M., Trickl, T., Wiegner,  
1104 M., Gerding, M., Mamouri, R. E., D'Amico, G., and Pappalardo, G.: Systematic lidar  
1105 observations of Saharan dust over Europe in the frame of EARLINET (2000-2002), *J.*  
1106 *Geophys. Res.*, 113, D10204, doi:10.1029/2007JD009028, 2008.

1107 Papayannis, A., Nicolae, D., Kokkalis, P., Biniotoglou, I., Talianu, C., Belegante, L.,  
1108 Tsaknakis, G., Cazacu, M. M., Vetres, I., and Ilic, L.: Optical, size and mass properties of  
1109 mixed type aerosols in Greece and Romania as observed by synergy of lidar and  
1110 sunphotometers in combination with model simulations: A case study, *Sci. Total Environ.*,  
1111 500-501, 277-294, doi:10.1016/j.scitotenv.2014.08.101, 2014.

1112 Pappalardo, G., Amodeo, A., Apituley, A., Comeron, A., Freudenthaler, V., Linné, H.,  
1113 Ansmann, A., Bösenberg, J., D'Amico, G., Mattis, I., Mona, L., Wandinger, U., Amiridis,  
1114 V., Alados-Arboledas, L., Nicolae, D., and Wiegner, M.: EARLINET: towards an advanced  
1115 sustainable European aerosol lidar network, *Atmos. Meas. Tech.*, 7, 2389-2409,  
1116 doi:10.5194/amt-7-2389-2014, 2014.

1117 Pérez, C., Nickovic, S., Pejanovic, G., Baldasano, J. M., and Özsoy, E.: Interactive dust-  
1118 radiation modeling: A step to improve weather forecasts. *J. Geophys. Res.*, 111, D16206,  
1119 doi:10.1029/2005JD006717, 2006a.

1120 Pérez, C., S. Nickovic, J. M. Baldasano, M. Sicard, F. Rocadenbosch and V. E. Cachorro  
1121 (2006a). A long Saharan dust event over the western Mediterranean: Lidar, Sun photometer  
1122 observations, and regional dust modeling, *J. Geophys. Res.*, 111, D15214,  
1123 doi:10.1029/2005JD006579, 2006b.

1124 Pérez, C., Haustein, K., Janjic, Z., Jorba, O., Huneus, N., Baldasano, J. M., Black, T.,  
1125 Basart, S., Nickovic, S., and Miller, R. L.: Atmospheric dust modeling from meso to global  
1126 scales with the online NMMB/BSC-Dust model–Part 1: Model description, annual  
1127 simulations and evaluation, *Atmos. Chem. Phys.*, 11, 13001-13027, doi:10.5194/acp-11-  
1128 13001-2011, 2011.

1129 Pérez-Ramírez, D., Navas-Guzmán, F., Lyamani, H., Fernández-Gálvez, J., Olmo, F. J.,  
1130 Alados-Arboledas, L.: Retrievals of precipitable water vapor using star photometry:  
1131 Assessment with Raman lidar and link to sun photometry, *J. Geophys. Res.*, 117, D05202,  
1132 doi:10.1029/2011JD016450, 2012.

1133 Perrone, M. R., De Tomasi, F., and Gobbi, G. P.: Vertically resolved aerosol properties by  
1134 multi-wavelength lidar measurements, *Atmos. Chem. Phys.*, 14, 1185-1204,  
1135 doi:10.5194/acp-14-1185-2014, 2014.

- 1136 Preißler, J., Wagner, F., Pereira, S. N., and Guerrero-Rascado, J. L. Multi-instrumental  
1137 observation of an exceptionally strong Saharan dust outbreak over Portugal, *J. Geophys.*  
1138 *Res.*, 116, D24204, doi:10.1029/2011JD016527, 2011.
- 1139 Remer, L. A., Kaufman, Y. J., Tanré, D., Mattoo, S., Chu, D. A., Martins, J. V., Li, R. R.,  
1140 Ichoku, C., Levy R. C., Kleidman R. G., Eck, T. F., Vermote, E., and Holben, B. N.: The  
1141 MODIS aerosol algorithm, products, and validation, *J. Atmos. Sci.*, 62, 947-973, 2005.
- 1142 Rodríguez, S., Alastuey, A., Alonso-Pérez, S., Querol, X., Cuevas, E., Abreu-Afonso, J.,  
1143 Viana, M., Pérez, N., Pandolfi, M., and Rosa, J.: Transport of desert dust mixed with North  
1144 African industrial pollutants in the subtropical Saharan Air Layer, *Atmos. Chem. Phys.*  
1145 *Disc.*, 11, 6663-6685, doi:10.5194/acp-11-6663-2011, 2011.
- 1146 Schättler, U., Doms, G., Schraff, C., 2008, A Description of the Nonhydrostatic Regional  
1147 COSMO-Model. Deutscher Wetterdienst, Offenbach. <http://www.cosmo-model.org>.
- 1148 Schepanski, K., Tegen, I., and Macke, A.: Saharan dust transport and deposition towards  
1149 the tropical northern Atlantic, *Atmos. Chem. Phys.*, 9, 1173-1189, doi:10.5194/acp-9-1173-  
1150 2009, 2009.
- 1151 Schepanski, K., Tegen, I., Laurent, B., Heinold, B., and Macke, A.: A new Saharan dust  
1152 source activation frequency map derived from MSG-SEVIRI IR-channels, *Geophys. Res.*  
1153 *Lett.*, 34, L18803, doi:10.1029/2007GL030168, 2007.
- 1154 Shimizu, A., Sugimoto, N., Matsui, I., Arao, K., Uno, I., Murayama, T., Kagawa, N., Aoki,  
1155 K., Uchiyama, A., and Yamazaki, A.: Continuous observations of Asian dust and other  
1156 aerosols by polarization lidars in China and Japan during ACE-Asia, *J. Geophys. Res.*,  
1157 109, D19S17, doi:10.1029/2002JD003253, 2004.
- 1158 Sicard, M., d'Amico, G., Comerón, A., Mona, L., Alados-Arboledas, L., Amodeo, A.,  
1159 Baars, H., Belegante, L., Biniotoglou, I., Bravo-Aranda, J. A., Fernández, A. J., Fréville, P.,  
1160 Garcia-Vizcaino, D., Giunta, A., Granados-Muñoz, M. J., Guerrero-Rascado, J. L.,  
1161 Hadjimitsis, D., Haeefe, A., Hervo, M., Iarlori, M., Kokkalis, P., Lange, D., Mamouri, R.  
1162 E., Mattis, I., Molero, F., Montoux, N., Muñoz, A., Muñoz-Porcar, C., Navas-Guzmán, F.,  
1163 Nicolae, D., Nisantzi, A., Papagiannopoulos, N., Papayannis, A., Pereira, S., Preißler, J.,  
1164 Pujadas, M., Rizi, V., Rocadenbosch, F., Sellegri, K., Simeonov, V., Tsaknakis, G.,  
1165 Wagner, F., and Pappalardo, G.: EARLINET: potential operationality of a research  
1166 network, *Atmos. Meas. Tech. Discuss.*, 8, 6599-6659, doi:10.5194/amtd-8-6599-2015,  
1167 2015.
- 1168 Sokolik, I. N., and Toon, O. B.: Incorporation of mineralogical composition into models of  
1169 the radiative properties of mineral aerosol from UV to IR wavelengths, *J. Geophys. Res.*,  
1170 104, 9423-9444.
- 1171 Spyrou, C., Mitsakou, C., Kallos, G., Louka P., and Vlastou, G.: An improved limited area  
1172 model for describing the dust cycle in the atmosphere, *J. Geophys. Res.*, 115, D17211,  
1173 doi:10.1029/2009JD013682, 2010.
- 1174 Takamura, T., and Nakajima, T.: Overview of SKYNET and its activities, *Opt. Pura Apl.*,  
1175 37, 3303-3308, 2004.
- 1176 Tegen, I., Schepanski, K., and Heinold, B.: Comparing two years of Saharan dust source  
1177 activation obtained by regional modeling and satellite observations, *Atmos. Chem. Phys.*,  
1178 13, 2381-2390, doi:10.5194/acp-13-2381-2013, 2013.

1179 Textor, C., Schulz, M. Guibert, S., Kinne, S., Balkanski, Y., Bauer, S., Berntsen, T.,  
1180 Berglen, T., Boucher, O., and M. Chin, M.: The effect of harmonized emissions on aerosol  
1181 properties in global models—an AeroCom experiment, *Atmos. Chem. Phys.*, 7, 4489-4501,  
1182 doi:10.5194/acp-7-4489-2007, 2007.

1183 Tsekeri, A., Amiridis, V., Kokkalis, P., Basart, S., Chaikovsky, A., Dubovik, O.,  
1184 Papayannis, A., Baldasano, J. M., and Gross, B.: Application of a synergetic lidar and  
1185 sunphotometer algorithm for the characterization of a dust event over Athens, Greece,  
1186 *British J. Environ. Clim. Change*, 3, 531-546,  
1187 doi:10.9734/BJECC/2013/2615#sthash.YeD42fFe.dpuf, 2013.

1188 Valenzuela, A., Olmo, F. J., Lyamani, H., Antón, M., Quirantes, A., and Alados-Arboledas,  
1189 L.: Classification of aerosol radiative properties during African desert dust intrusions over  
1190 southeastern Spain by sector origins and cluster analysis, *J. Geophys. Res.*, 117, D06214,  
1191 doi:10.1029/2011JD016885, 2012.

1192 Valenzuela, A., Olmo, F. J., Lyamani, H., Granados-Muñoz, M. J., Antón, M., Guerrero-  
1193 Rascado, J. L., Quirantes, A., Toledano, C., Perez-Ramírez, D., and Alados-Arboledas, L.:  
1194 Aerosol transport over the western Mediterranean basin: Evidence of the contribution of  
1195 fine particles to desert dust plumes over Alborán Island, *J. Geophys. Res.*, 119, 14028-  
1196 14044, doi:10.1002/2014JD022044, 2014.

1197 Vukovic, A., M. Vujadinovic, G. Pejanovic, J. Andric, M. J. Kumjian, V. Djurdjevic, M.  
1198 Dacic, A. K. Prasad, H. M. El-Askary, B. C. Paris, S. Petkovic, W. Sprigg, and S.  
1199 Nickovic: Numerical Simulation of “An American Haboob”, *Atmos. Chem. Phys.*, 14,  
1200 3211-3230, doi: 10.5194/acp-14-3211-201, 2014.

1201 Wagner, J., A. Ansmann, U. Wandinger, P. Seifert, A. Schwarz, M. Tesche, A. Chaikovsky  
1202 and Dubovik, O.: Evaluation of the Lidar/Radiometer Inversion Code (LIRIC) to determine  
1203 microphysical properties of volcanic and desert dust, *Atmos. Meas. Tech.*, 6, 1707-1724,  
1204 doi:10.5194/amt-6-1707-2013, 2013.

1205 Wang, Y., Sartelet, K. N., Bocquet, M., Chazette, P., Sicard, M., D'Amico, G., Léon, J. F.,  
1206 Alados-Arboledas, L., Amodeo, A., Augustin, P., Bach, J., Belegante, L., Biniotoglu, I.  
1207 Bush, X., Comerón, A., Delbarre, K., García-Vízcaino, D., Guerrero-Rascado, J.-L., Hervo,  
1208 M., Iorli, M., Kokkalis, P., Lange, D., Molero, F., Montoux, N., Muñoz, A., Muñoz, C.,  
1209 Nicolae, D., Papayannis, A., Pappalardo, G., Preissler, J., Rizi, V., Rocadenbosch, F.,  
1210 Sellegri, K., Wagner, F., and Dulac, F.: Assimilation of lidar signals: application to aerosol  
1211 forecasting in the western Mediterranean Basin. *Atmos. Chem. Phys.*, 14, 12031-12053,  
1212 doi:10.5194/acp-14-12031-2014, 2014.

1213 Welton, E. J., Campbell, J. R., Berkoff, T. A., Valencia, S., Spinhirne, J. D., Holben, B.,  
1214 and Tsay, S.C.: 5.2 The Nasa Micro-Pulse Lidar Network (MPLNET): co-location of lidars  
1215 with AERONET sunphotometers and related Earth Science applications, *Proc. 85<sup>th</sup> Annu.*  
1216 *Meet. Am. Meteor. Soc.*, San Diego, 9–13 January 2005, 5165–5169, 2005.

1217 Wolke, R., Schroeder, W., Schroedner, R., and Renner, E.: Influence of grid resolution and  
1218 meteorological forcing on simulated European air quality: A sensitivity study with the  
1219 modeling system COSMO-MUSCAT, *Atmos. Environ.*, 53, 110-130,  
1220 doi:10.1016/j.atmosenv.2012.02.085, 2012.

1221 Zender, C. S., Miller, R., and I. Tegen, I: Quantifying mineral dust mass budgets:  
1222 Terminology, constraints, and current estimates, *Eos, Trans. Am. Geophys. Un.*, 85, 509-  
1223 512, doi:10.1029/2004EO480002, 2004.  
1224

1225 Tables:

1226

1227

1228

1229

1230

1231

Table 1. Lidar and sun-photometer characteristics for the five stations considered in this study and depicted in Figure 1. A more detailed description of the experimental sites and the lidar systems in every station can be found in the references included in Reference column of the table.

Site	Latitude, Longitude	Altitude (m asl)	Lidar characteristics			Sun-photometer characteristics	Reference
			Elastic channels (nm)	Raman channels (nm)	System name	Channels (nm)	
AT (Athens)	37.97°N, 23.77°E	200	355, 532, 1064	387,407,607	EOLE	340,380,440,500, 675,870,1020,1640	[Kokkalis et al., 2012]
BA (Barcelona)	41.39°N, 2.17°E	115	355, 532, 1064	387,407,607	UPCLidar	440,675,870,1020	[Kumar et al., 2011]
BU (Bucharest)	44.35°N, 26.03°E	93	355, 532 parallel, 532 cross, 1064	387,407,607	RALI (LR313 - D400)	340,380,440,500, 675,870,1020	[Nemuc et al., 2013]
EV (Évora)	38.57°N, 7.91°W	293	355, 532, 532 cross, 1064	387,407,607	PAOLI	340,380,440,500, 675,870,1020,1640	[Preißler et al., 2011]
GR (Granada)	37.16°N, 3.61°W	680	355, 532 parallel, 532 cross, 1064	387,407,607	MULHACEN (LR321-D400)	340,380,440,500, 675,870,1020	[Guerrero-Rascado et al., 2009]

1232

1233

1234

1235

1236

1237

*Table 2. Summary of the main parameters of the mineral dust transport models used in this study.*

	<b>BSC-DREAM8b</b>	<b>NMMB/BSC-Dust</b>	<b>COSMO-MUSCAT</b>	<b>DREAM8-NMME</b>
Institution	BSC-CNS	BSC-CNS	TROPOS	SEEVCCC/IPB
Meteorological driver	Eta/NCEP	NMMB/NCEP	COSMO	NMME/NCEP
Initial and boundary conditions	NCEP/FNL	NCEP/FNL	GME	ECMWF analysis data in 6-hour intervals
Domain	30°W to 65°E and 0°N to 65°N	30°W to 65°E and 0°N to 65°N	30°W to 35°E and 0°N to 60°N	221x251 points, 26W, 62E, 7N, 57N
Resolution	0.33°× 0.33°	0.33°× 0.33°	0.25°× 0.25°	0.2°× 0.2°
Vertical resolution	24 Eta-layers	40 $\sigma$ -hybrid layers	41 $\sigma$ -hybrid layers	28 $\sigma$ -hybrid pressure levels
Radiation interaction	Yes	No activated	Yes, online	No
Data assimilation	No	No	No	No



1238

1239 Table 3.  $\tau_{440\text{nm}}$  and AE(440-870nm) daily mean values (+ standard deviation) at the five  
1240 stations on 9<sup>th</sup>, 10<sup>th</sup> and 11<sup>th</sup> of July 2012.

1241

1242

Site	9 July		10 July		11 July	
	$\tau_{440\text{nm}}$	AE(440-870nm)	$\tau_{440\text{nm}}$	AE(440-870nm)	$\tau_{440\text{nm}}$	AE(440-870nm)
AT	0.51±0.02	1.76±0.01	0.45±0.0	1.67±0.03	0.44±0.01	1.28±0.02
BA	n/d	n/d	0.28±0.0	1.65±0.05	0.27±0.03	1.47±0.01
BU	0.40±0.04	1.08±0.04	0.34±0.0	1.07±0.06	0.62±0.05	1.10±0.05
EV	0.08±0.02	0.82±0.12	0.08±0.0	0.87±0.12	0.08±0.02	0.90±0.09
GR	0.28±0.03	0.32±0.05	0.12±0.0	0.60±0.30	0.11±0.02	0.60±0.10

1243

1244

1245

1246

1247 Figure captions:

1248 *Figure 1. Stations where LIRIC algorithm was been applied during ChArMEEx/EMEP 2012 intensive*  
1249 *measurement period on 9th-11th of July. Source: Google Earth.*

1250 *Figure 2. a) AERONET Level 1.5 retrieved  $\tau_{440nm}$  and b) AE(440-870nm) during CHARMEX 2012*  
1251 *campaign at the five stations(see Table 1 for station descriptions). c) AERONET Version 2 Level 1.5 size*  
1252 *distributions retrieved for 9<sup>th</sup>, 10<sup>th</sup> and 11<sup>th</sup> July. n/d indicates no data availability.*

1253 *Figure 3. RCS at 532 nm (1064nm at Athens) in arbitrary units for the five stations during ChArMEEx*  
1254 *2012 measurements campaign.*

1255 *Figure 4. Volume concentration profiles of the total coarse mode and the fine mode at Barcelona and*  
1256 *Athens, and volume concentration profiles of fine, coarse spherical and coarse spheroid mode at Évora ,*  
1257 *Bucharest and Granada (from left to right) for different periods of the 9<sup>th</sup>, 10<sup>th</sup> and 11<sup>th</sup> of July 2012*  
1258 *(from top to bottom).*

1259 *Figure 5. MODIS FIRMS image indicating the active fires during the five previous days to the 11<sup>th</sup> July*  
1260 *2012. The red line correspond to the air-mass 5-day back-trajectory arriving over Bucharest at 3000 m*  
1261 *asl on 11<sup>th</sup> of July 2012.*

1262 *Figure 6. a) 5-day backward trajectories arriving over Granada on 9<sup>th</sup>, 10<sup>th</sup> and 11<sup>th</sup> July 2012 at 12:00*  
1263 *UTC (from left to right) computed by HYSPLIT model. b) Locations of the main industrial activity in the*  
1264 *North of Africa (brown stars)taken from Rodriguez et al., [2011] together with the 5-day backwards*  
1265 *trajectories arriving at Granada experimental site on 9<sup>th</sup> July 2012 at 12:00 UTC.*

1266 *Figure 7. Time series of the volume concentration profiles (in  $\mu\text{m}^3/\text{cm}^3$ ) for the fine mode (upper part),*  
1267 *coarse spherical mode (middle part) and coarse spheroid mode (lower part) for days 9<sup>th</sup>, 10<sup>th</sup> and 11<sup>th</sup>*  
1268 *July 2012 (from left to right).*

1269 *Figure8. Time series of the  $\delta^p_{532nm}$  profiles retrieved from Granada lidar system at different time*  
1270 *intervals during during ChArMEEx July 2012 intensive measurement period. Dark blue color represents*  
1271 *regions and time periods where no data were retrieved.*

1272 *Figure 9.  $\tau_{550nm}$  from MODIS/Terra (top) and  $\tau_{675nm}$  daytime mean from MSG-SEVIRI (bottom) on*  
1273 *9th, 10th and 11th of July.*

1274 *Figure 10.  $\tau_{550nm}$  forecast by a) BSC-DREAM8b, b) DREAM8-NMME c) NMMB/BSC-Dust and d)*  
1275 *COSMO-MUSCAT models for 9th, 10th and 11th July 2012 at 12:00 UTC over Europe and North Africa.*  
1276 *The yellow stars represent the location of the stations where microphysical properties profiles are*  
1277 *retrieved with LIRIC.*

1278 *Figure 11. Dust mass concentration profiles obtained with LIRIC (dotted line) and BSC-DREAM8b-v2,*  
1279 *DREAM8-NMME, DREAMABOL, NMMB/BSC-Dust for Granada station every three hours on 9<sup>th</sup>, 10<sup>th</sup> and*  
1280 *11<sup>th</sup> of July 2012.*

1281 *Figure 12. (from top to bottom)Time series of the integrated mass concentration values (above 2 km in*  
1282 *altitude) retrieved from LIRIC and the four evaluated models vertical profiles for the period between*  
1283 *15:00 UTC on 9<sup>th</sup> of July 2012 and 18:00 UTC on 11<sup>th</sup> of July 2012. Time series of the correlation*  
1284 *coefficient R, between LIRIC-derived mass concentration profiles and each one of the four evaluated*  
1285 *models for the same period. Time series of the dust center of mass,  $C_m$ , obtained from LIRIC and the*  
1286 *models profiles.*

1287 *Figure 13. Vertical profiles of the correlation coefficient between LIRIC and the models time series for*  
1288 *every altitude level, the root mean square error RMSE, the normalized mean bias NMB and the*  
1289 *normalized mean standard deviation NMSD.*

1290

1291 Figures:



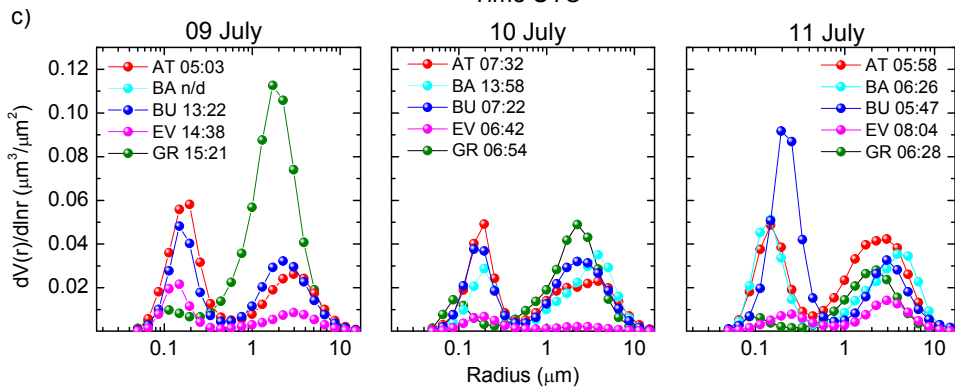
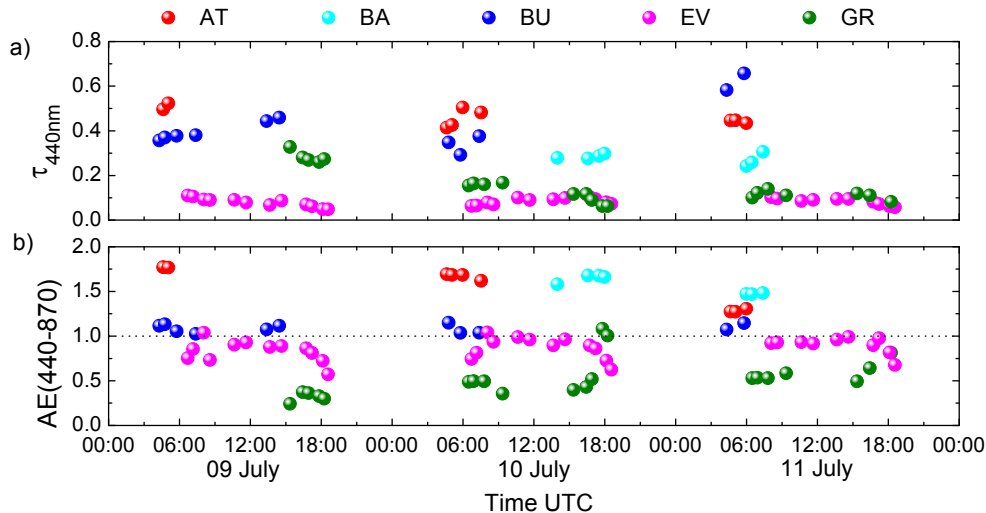
Bucharest

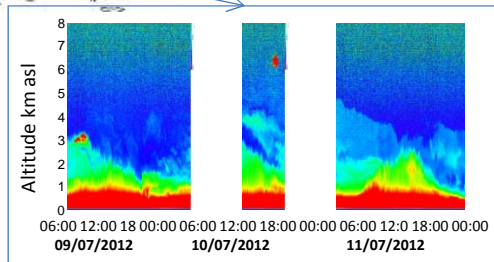
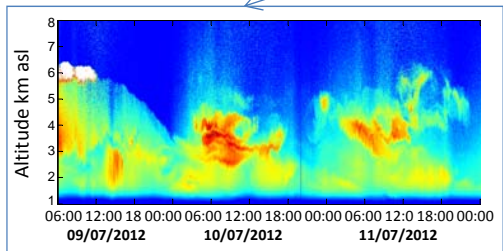
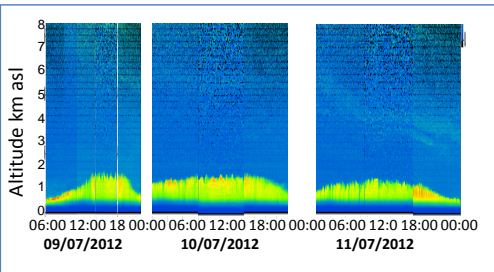
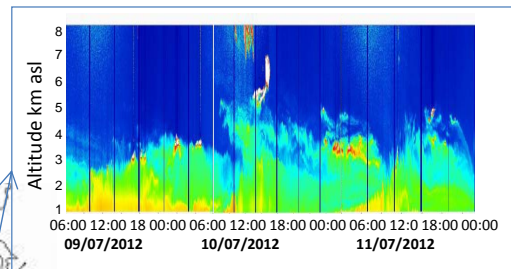
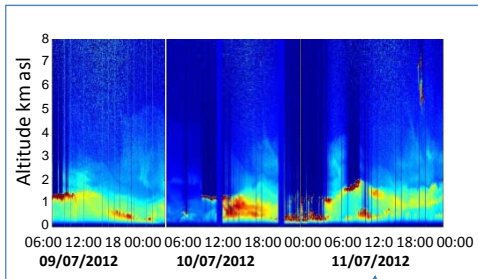
Barcelona

Evora

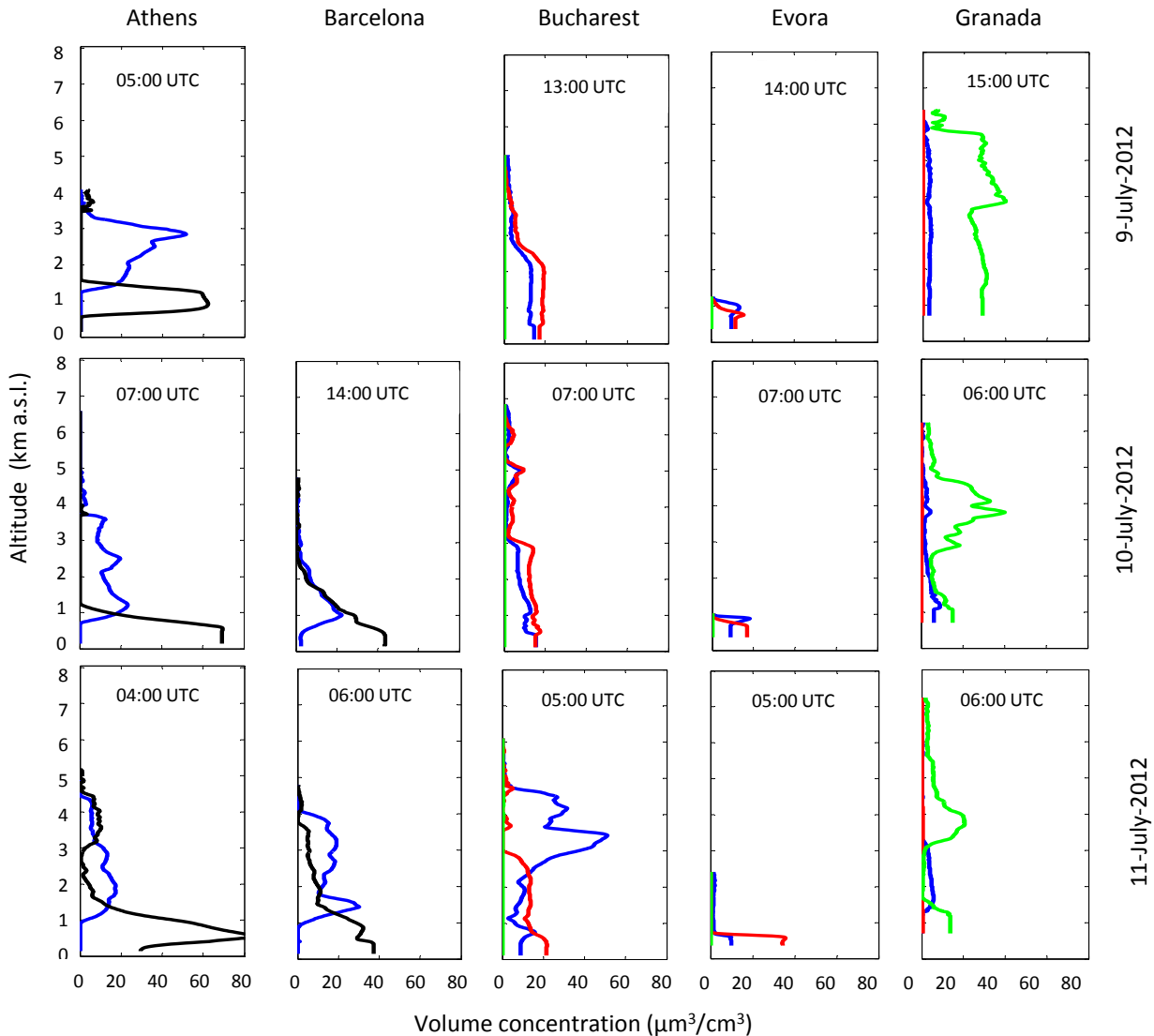
Granada

Athens





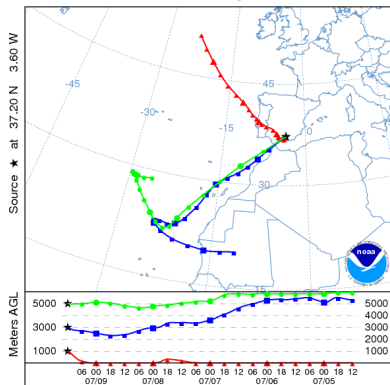
Fine mode CSpherical mode CSpheroid mode Coarse mode



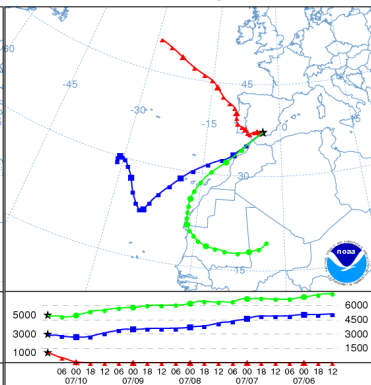


a)

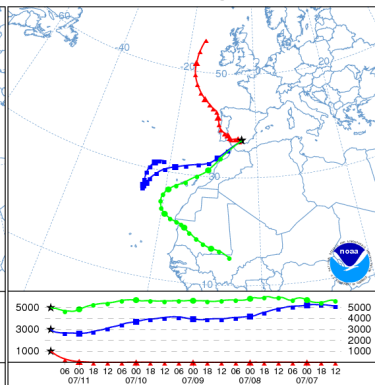
NOAA HYSPLIT MODEL  
Backward trajectories ending at 1200 UTC 09 Jul 12  
GDAS Meteorological Data



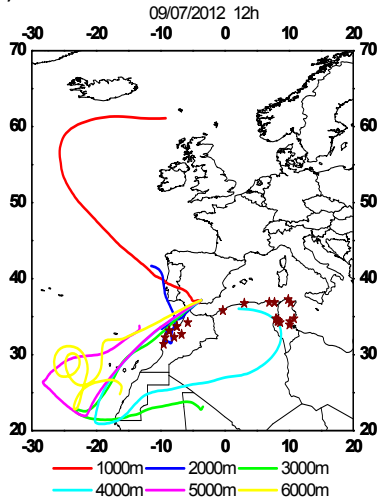
NOAA HYSPLIT MODEL  
Backward trajectories ending at 1200 UTC 10 Jul 12  
GDAS Meteorological Data



NOAA HYSPLIT MODEL  
Backward trajectories ending at 1200 UTC 11 Jul 12  
GDAS Meteorological Data



b)

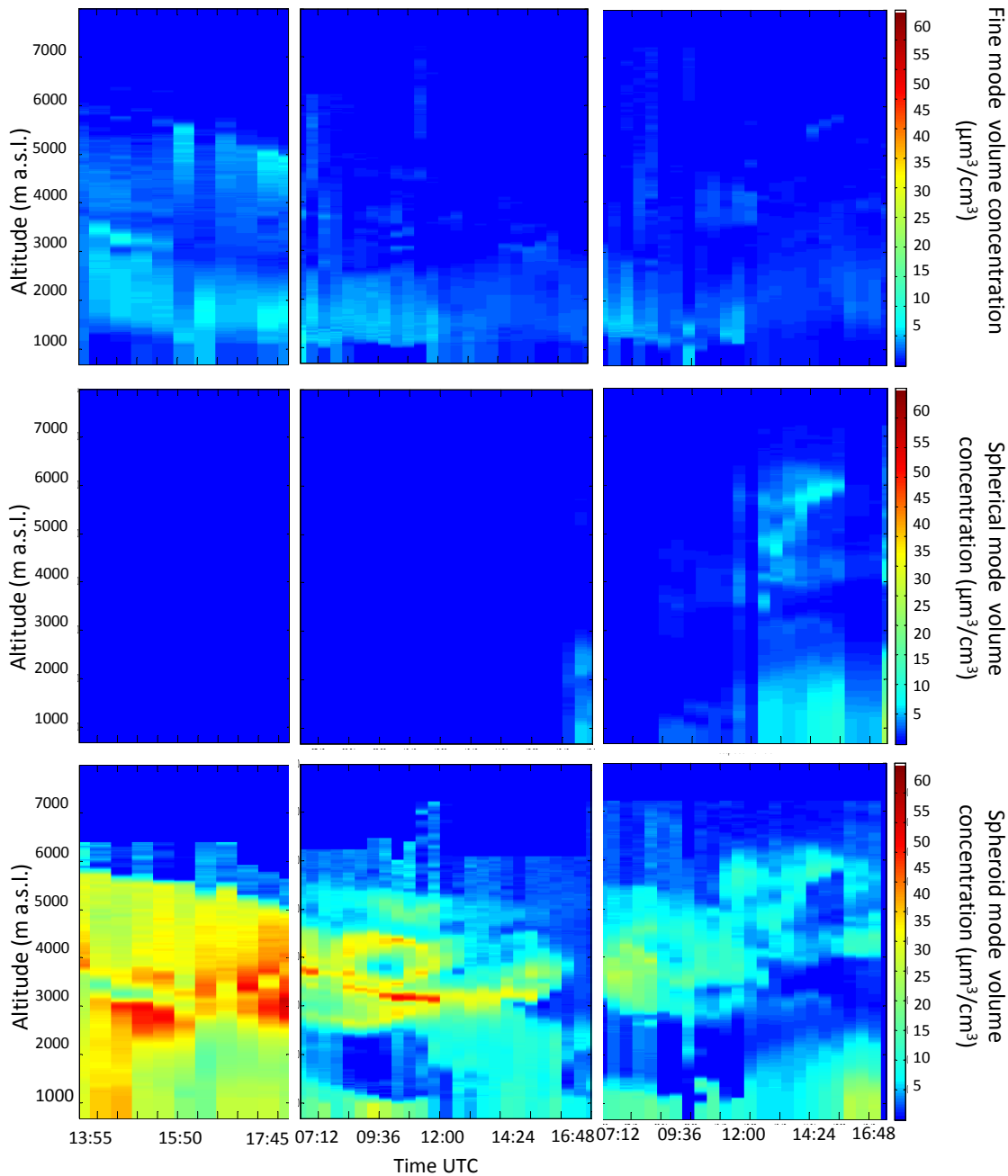


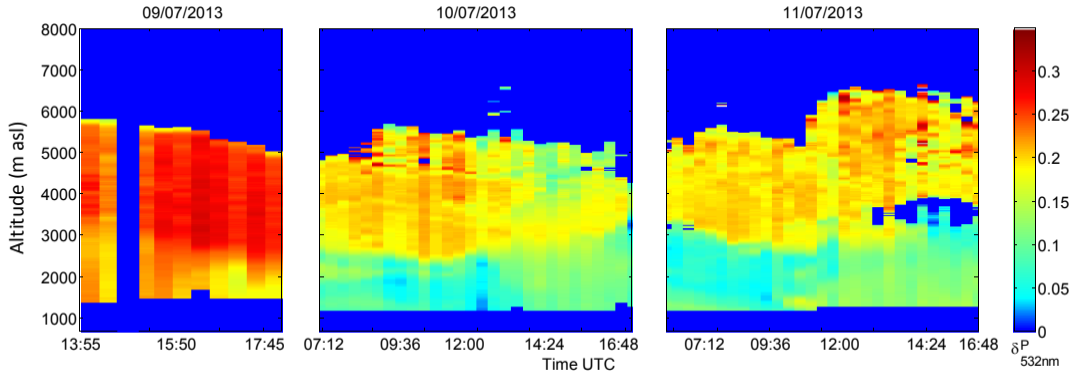


09/07/2012

10/07/2012

11/07/2012





9 July 2012

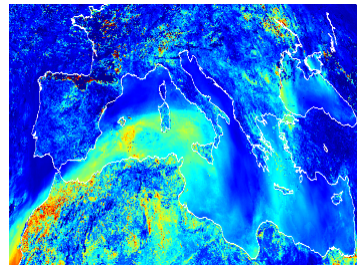
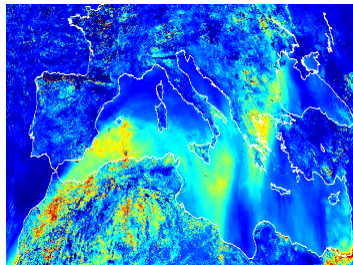
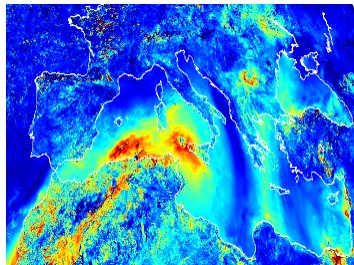
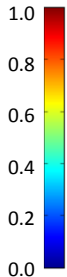
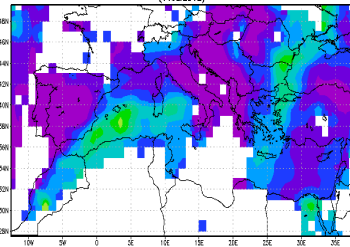
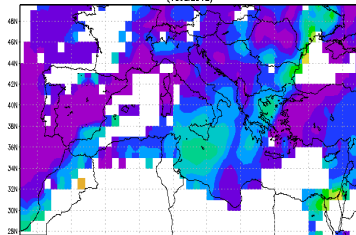
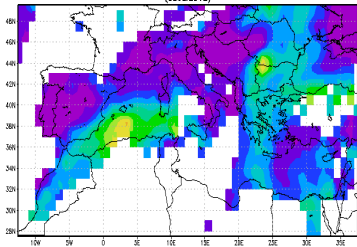
10 July 2012

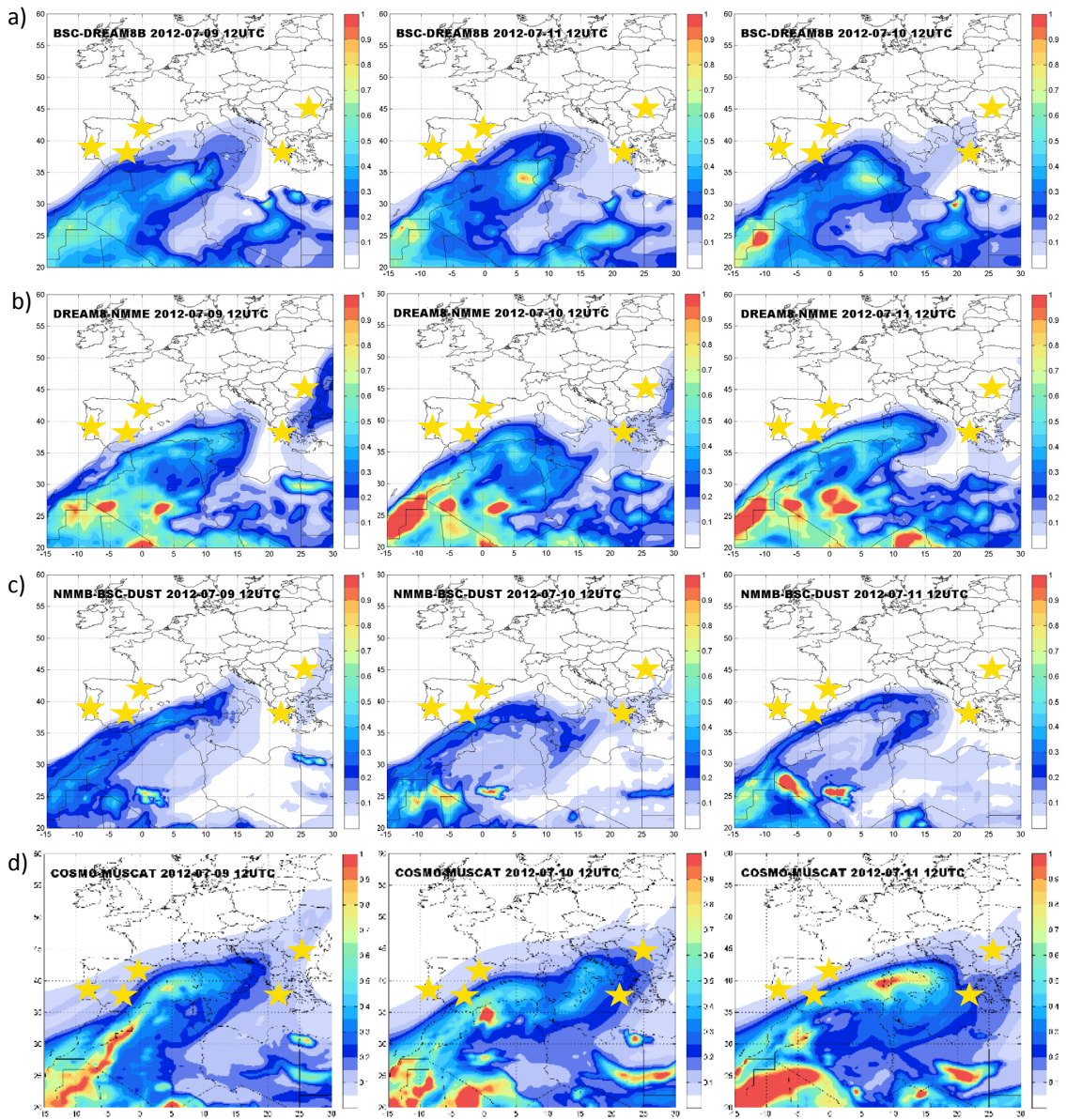
11 July 2012

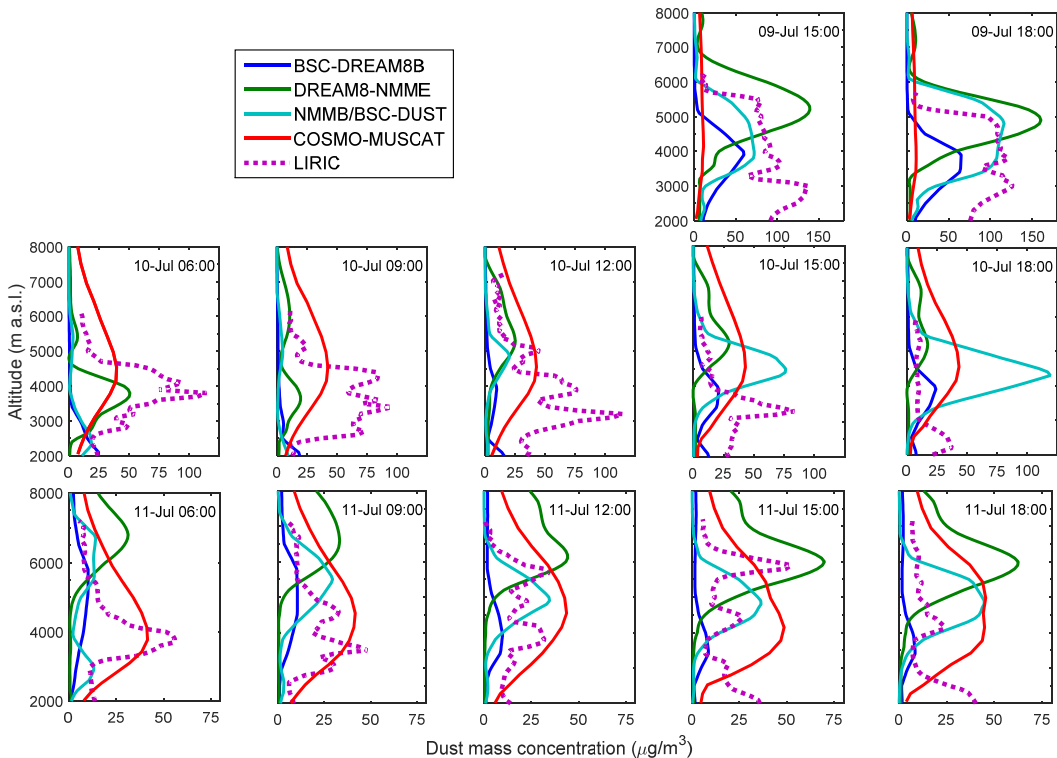
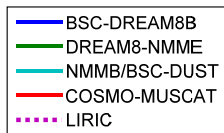
MOD08\_D3.051 Aerosol Optical Depth at 550 nm [unitless]  
(09Jul2012)

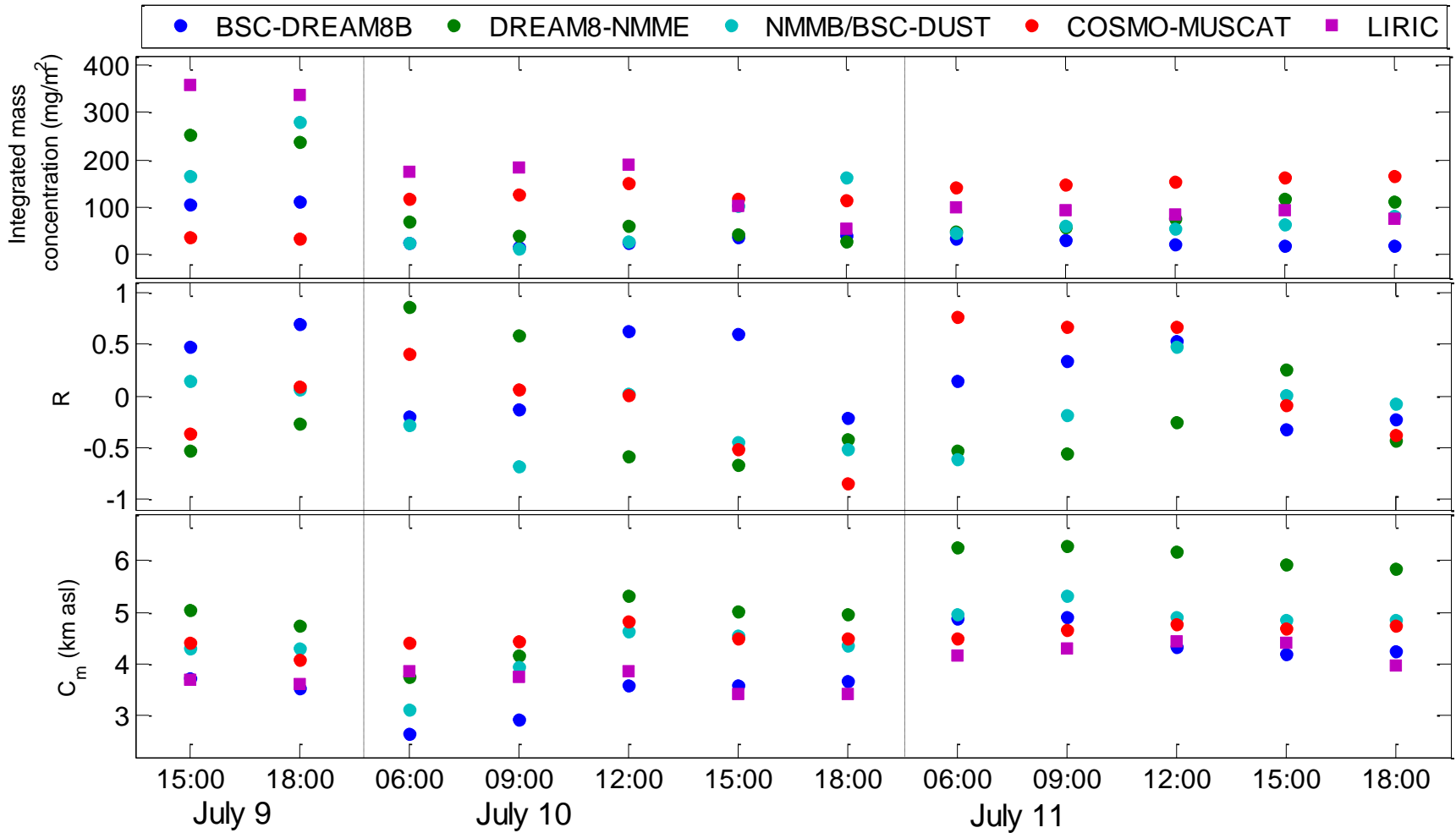
MOD08\_D3.051 Aerosol Optical Depth at 550 nm [unitless]  
(10Jul2012)

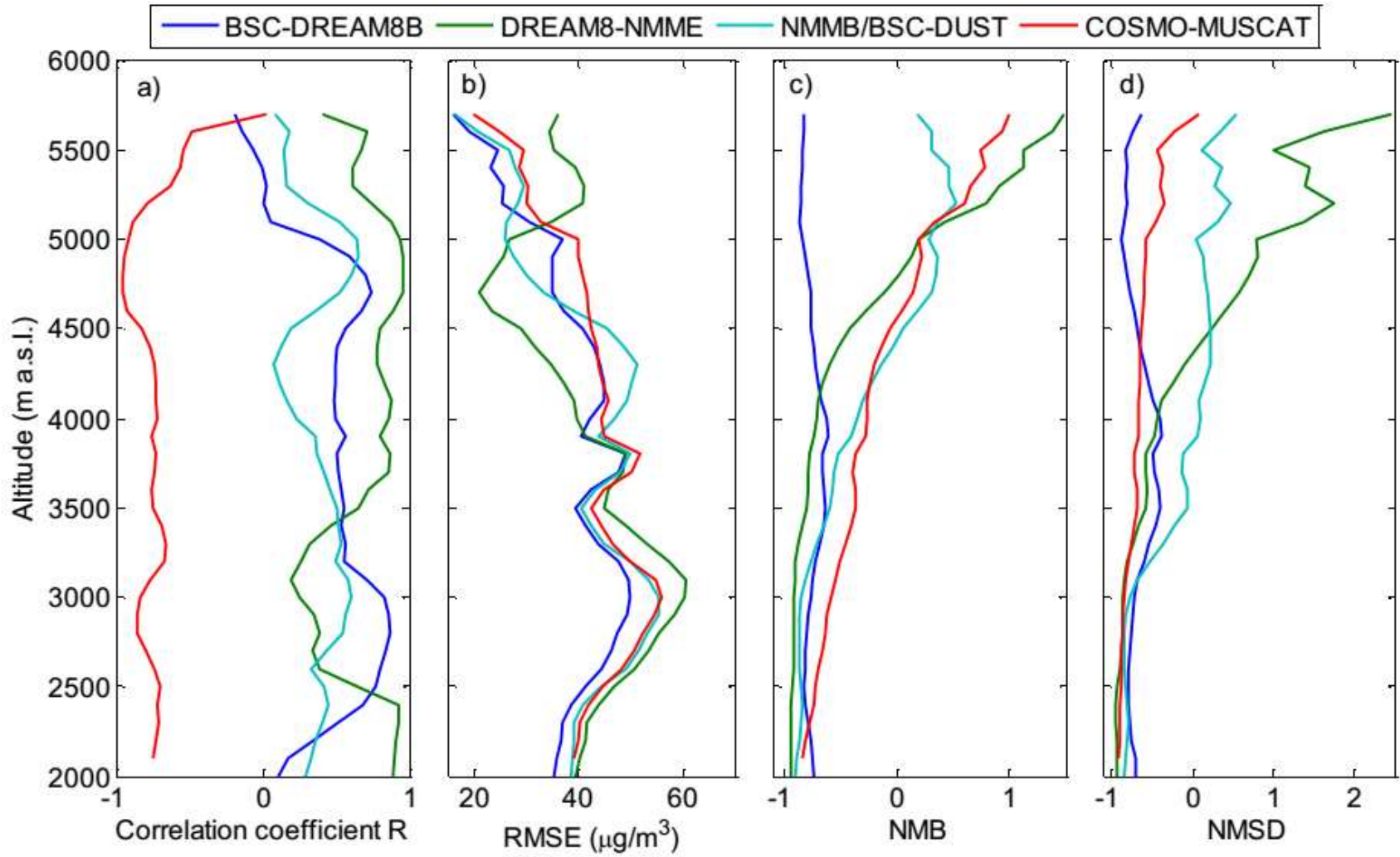
MOD08\_D3.051 Aerosol Optical Depth at 550 nm [unitless]  
(11Jul2012)











Supplementary material:

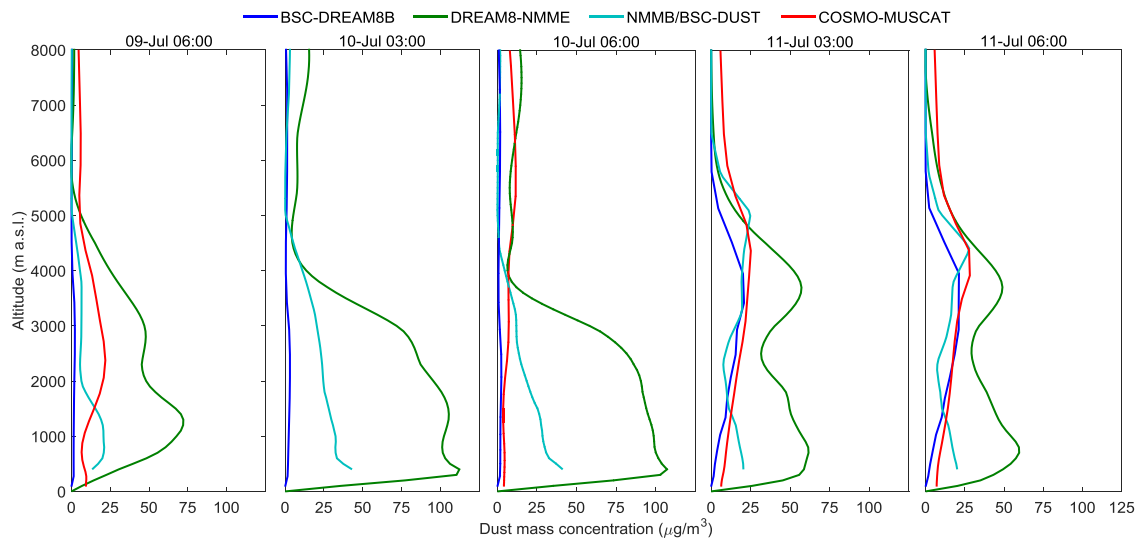


*Figure S1. Dust mass concentration profiles forecast by BSC-DREAM8b-v2, DREAM8-NMME, NMMB/BSC-Dust and COSMO-MUSCAT at Athens in the period 9 July 2012-11 July 2012. Only those data coincident with AERONET inversion retrievals ( $\pm 3$  hours) has been presented here.*



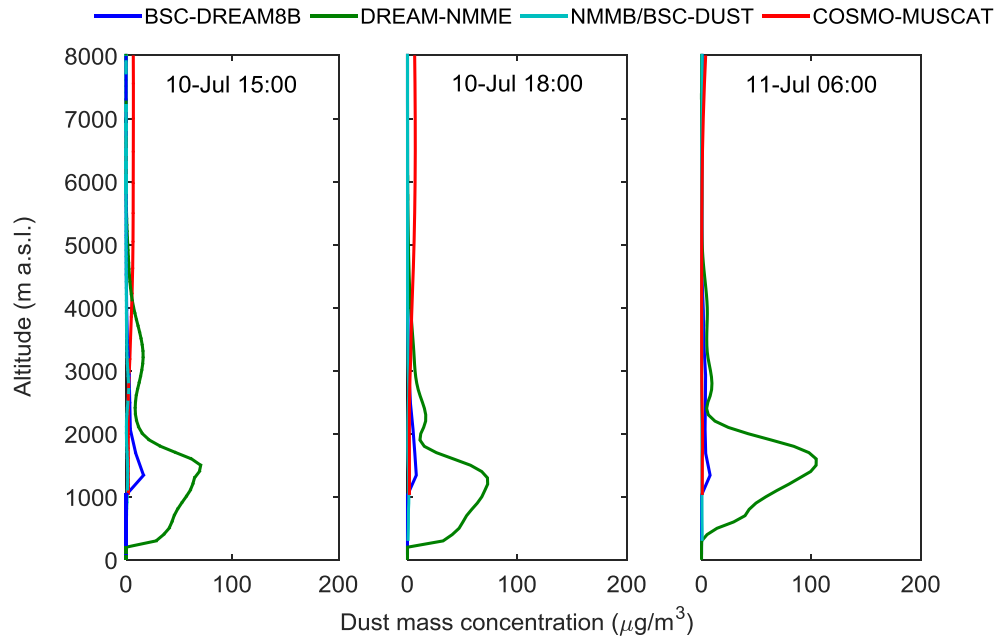


*Figure S2. Dust mass concentration profiles forecast by BSC-DREAM8b-v2, DREAM8-NMME, DREAMABOL and NMMB/BSC-Dust at Barcelona in the period 9 July 2012-11 July 2012. Only those data coincident with AERONET inversion retrievals ( $\pm 3$  hours) has been presented here.*

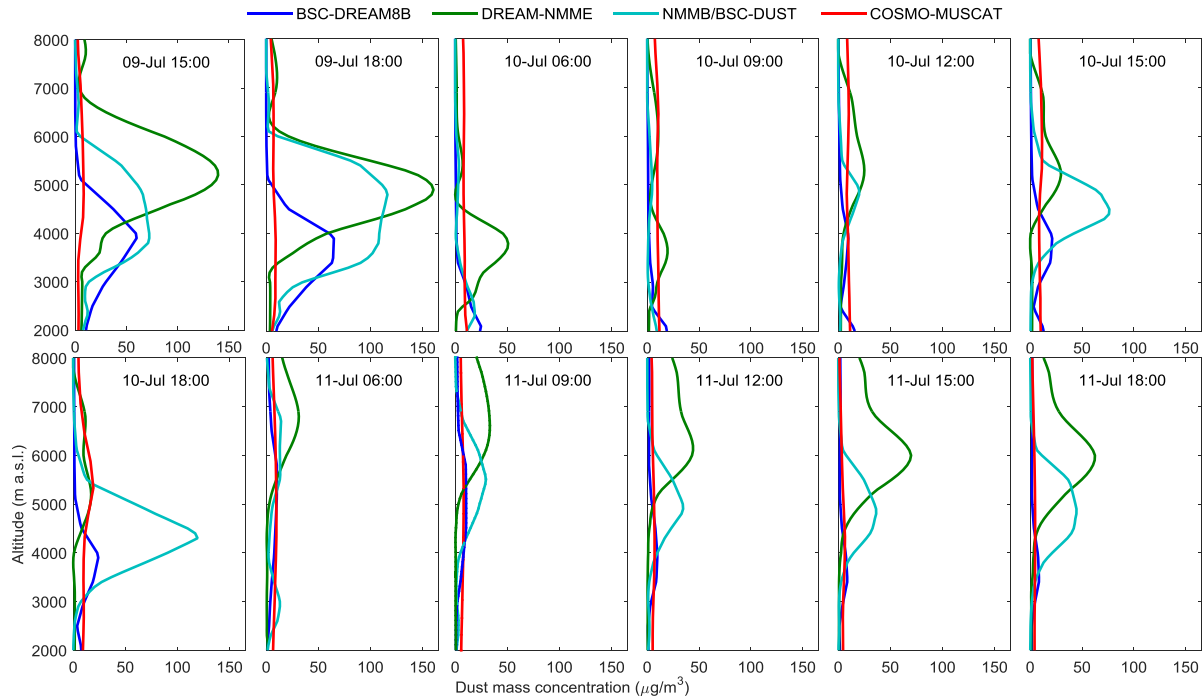


*Figure S3. Dust mass concentration profiles forecast by BSC-DREAM8b-v2, DREAM8-NMME, NMMB/BSC-Dust and COSMO-MUSCAT at Bucharest in the period 9 July 2012-11 July 2012. Only those data coincident with AERONET inversion retrievals ( $\pm 3$  hours) has been presented here.*

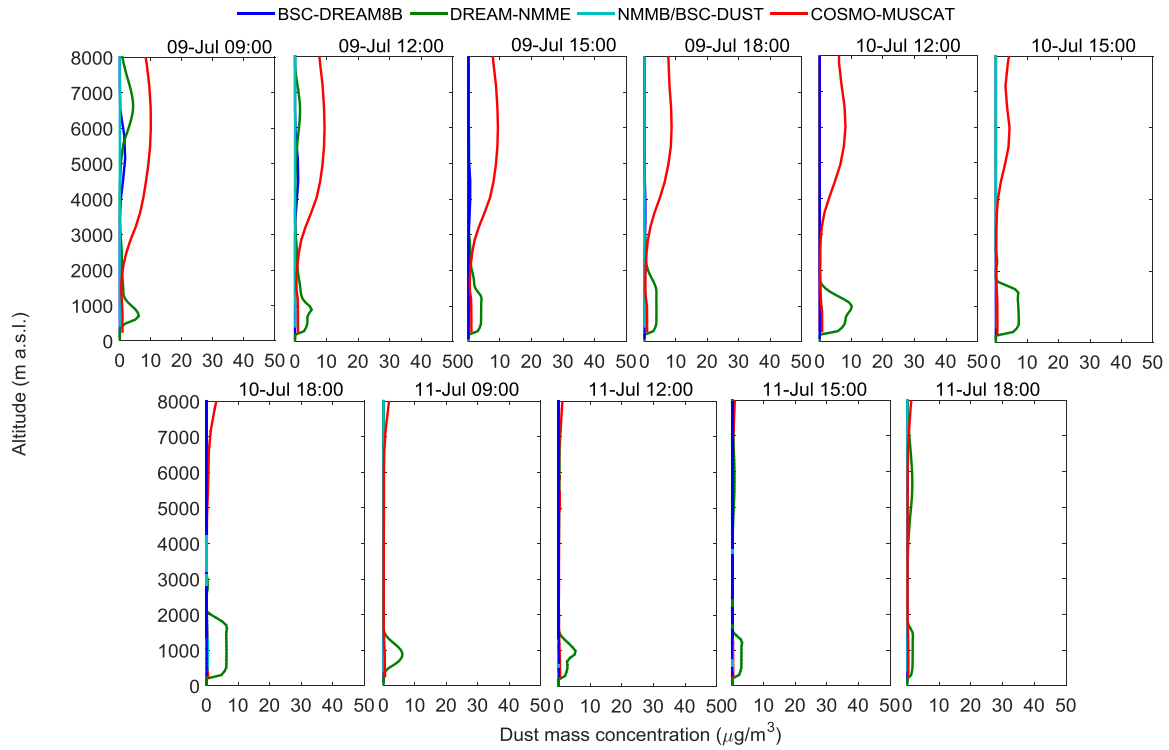


Figure S4. Dust mass concentration profiles forecast by BSC-DREAM8b-v2, DREAM8-NMME, NMMB/BSC-Dust and COSMO-MUSCAT at Évora in the period 9 July 2012-11 July 2012. Only those data coincident with AERONET inversion retrievals ( $\pm 3$  hours) has been presented here.

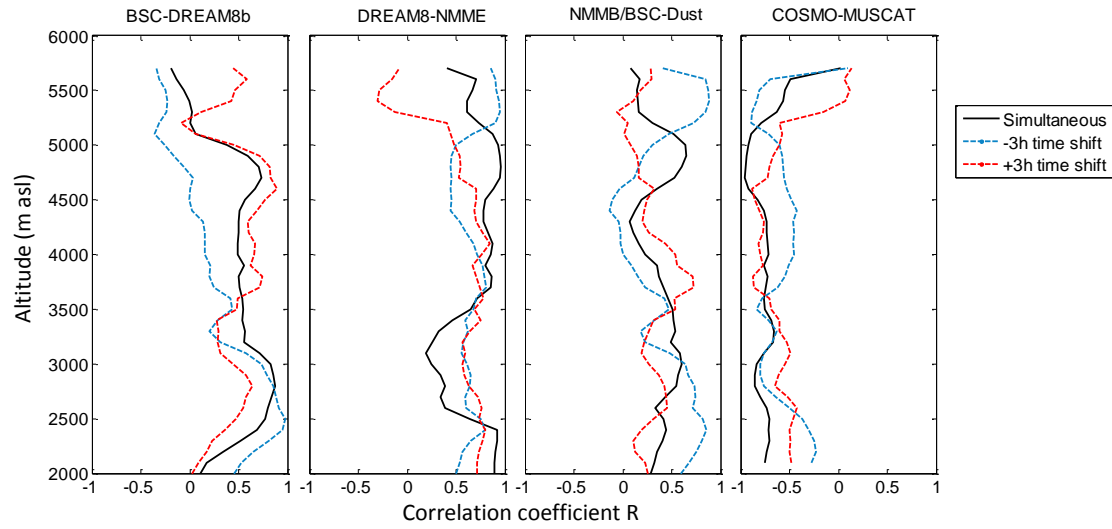


Figure S5. Correlation coefficient  $R$  between simultaneous LIRIC and modelled time series (solid black lines) for every altitude level. Dashed lines represent  $R$  values obtained for the modelled time series and LIRIC time series with a time shift of plus (red line) and minus (blue line) 3 hours.